Characterizing diffusive growth by uncertainty quantification

Paul Pukite, Steve Bankes, Dan Challou
BAE Systems

Abstract: Environmental models of growth processes contain a great deal of uncertainty. Since the underlying process behavior is rarely well-ordered, any model characteristics will carry along with it a level of aleatory uncertainty governed by the natural disorder. This paper applies novel uncertainty quantification approaches to classes of diffusion problems which illustrate the benefit of assuming natural variability, such as varying rates of oxidation and corrosion.

Introduction

Modeling with uncertainty quantification has application to such phenomena as oxidation, corrosion, thermal response, and particulate growth. These fall into the classes of phenomena governed substantially by diffusional processes. At its most fundamental, diffusion is a model of a random walk. Without a strong convection or advection term to guide the process (e.g. provided by an electric or gravitational field), the kinetic mechanism of a particle generates a random trajectory that is well understood based on statistical physics principles. The standard physics approach is to solve a master diffusion equation under transient conditions. This turns into a kernel solution that we can apply to an arbitrary forcing function, such as provided by an input material flux or thermal impulse.

Yet, the environment that the particle resides in may not be as homogeneous as the ideal diffusion model would imply. Enough uncertainty in the essential diffusion parameters may exist that we need to ask some fundamental questions:

- Why do we assume the diffusion coefficient is a constant?
- How can we know the diffusional interface so precisely?

Within a heterogeneous media, the characteristic diffusion coefficient does not have to remain a fixed value. Varying material composition and amounts of defects can modulate the natural hopping rate and thus smear the diffusion coefficient well beyond the narrow tolerance that is typically assumed. In general, the assumption of a single diffusion coefficient works well for many behaviors ─ as the observed results are already smeared due to diffusion, while a greater level of uncertainty will not change the mean value of the diffused measures. This mean value approximation works well as a result of applying the central limit theorem of statistics.

Yet, under certain circumstances, the uncertainty in the diffusion coefficient or uncertainty in the experimental geometry will have a subtle yet measurable impact on the diffusional transient behavior. This departure from ideality usually occurs over the short initial growth time, but will also manifest itself via the application of a modified impulse response function.

As an example, if we consider the heat equation, which models the thermal evolution of a transient heat impulse, we immediately note that the standard solution admits an infinite speed of propagation of the initial thermal transient, due to a singularity in the kernel solution expression. That first random walk step is instantaneous according to the math, yet we need to either integrate this transient out or invoke a model such as relativistic diffusion [1][2] to account for the real system behavior. Furthermore, *and just as*

plausibly, the initial transient is likely modified by unaccounted natural uncertainty and disorder in the thermal characteristics and environment, i.e. within the *thermal context*.

This uncertainty also manifests itself in other diffusion models. Deviations from the expected Fickian diffusional growth model lead to the Deal-Grove model[3] for Si oxide growth on a silicon wafer as a practical yet non-ideal heuristic.

In this paper, we apply straight-forward uncertainty quantification. The essential idea is to admit some uncertainty in the diffusion coefficient and in the interface location. By propagating the uncertainty into the diffusion response, certain issues disappear. For example, the infinite speed becomes finite and the kernel solution comes out very clean. This becomes part of the initial condition uncertainty that we know must exist in practice.

In the following work we apply two levels of uncertainty

- Vary the diffusion coefficient to maximum uncertainty with known mean
- Vary the diffusional interface to maximum uncertainty with known mean

As a result we generate a simple diffusion kernel that is much easier to reason with, and can explain several subtle anomalous diffusion behaviors

Example: SiO_2 growth

We first consider the well-known characterization of silicon dioxide, SiO2 as an example of dispersive growth. Originally characterized by Bruce Deal and Andrew Grove in the 1960's, a careful application of a diffusion-based oxide growth model partially enabled the semiconductor revolution. As illustrated in **Figure 1**, the Deal-Grove model works as a heuristic model in so far as a rigorous first-principles derivation does not exist.

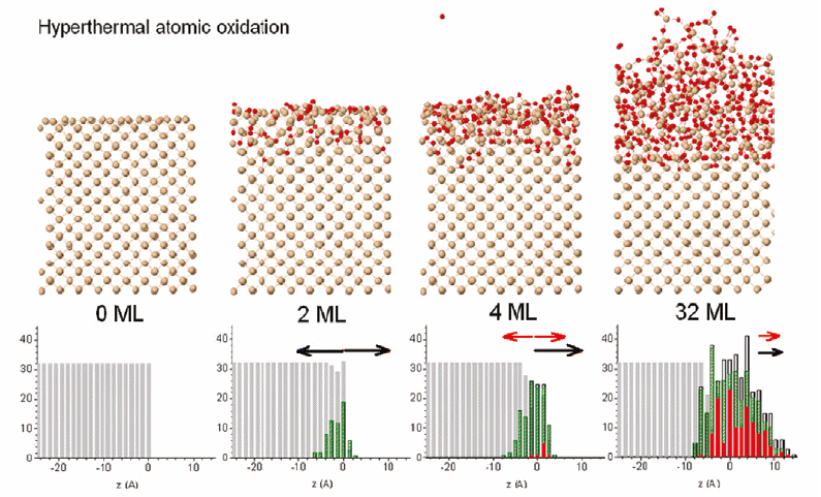

Figure 1: *Chemical simulation of oxidation of silicon. A large degree of disorder is evidenced by the mixture of pure Si, SiO_2, and SiO and as indicated in the histograms by light gray bars, green bars, and red bars, respectively. Black and red arrows indicate the growth direction of the oxidized and silica (SiO) layers, respectively (from [4])*

The following derivation improves on the Deal-Grove model by assuming that the diffusion coefficient and location of the growing oxide layer is smeared by a maximum entropy amount; i.e. we can estimate the mean but we leave higher-order moments to vary to maximize the entropy.

Diffusion Solution

The standard approach for solving diffusion problems starts from master diffusion equation

$$\frac{\partial}{\partial t}C(t,x) = D \cdot \frac{\partial^2}{\partial x^2}C(t,x) \tag{1}$$

also known as Fokker-Planck, this is a one-dimensional representation and only lacks the convective or drift term from the general formulation of Fokker-Planck. We also assume that *D* does not change with respect to spatial coordinates.

We can easily derive the solution of the response function if we think of the diffusion from a planar source outward. The kernel solution gives:

$$n(t,x|D) = \frac{1}{\sqrt{4\pi Dt}} \cdot e^{-x^2/4Dt} \tag{2}$$

We place an impulse of reactants at x=0 and want to watch the evolution of the concentration, *n*, with time. As the concentration drops, we assume that the diffused material from that amount contributes to the growth of the oxide layer.

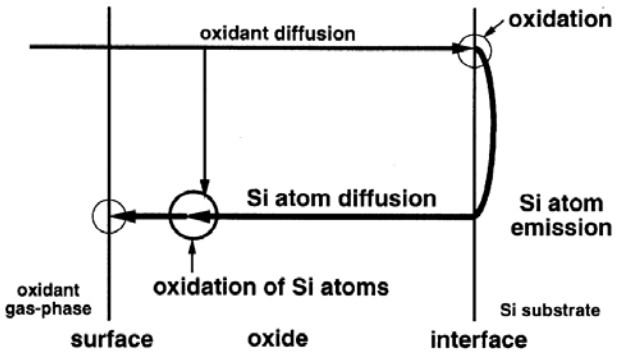

Figure 2: *Mechanism for diffusion (from [5])*

Consider first that the kernel function represents a one-dimensional concentration profile, in units of number of atomic elements per thickness. The expression *n(t,x)* describes how quickly the atomic concentration decreases from its initial value. So the accumulated concentration, representing the growth outward from the interface, is the spatial integral of the concentration density. Early on we assume that the region of the interface is spread over a width *X*.

$$N(t|X,D) = \int_0^X n(t,x|D)dx \tag{3}$$

The average flux of atoms outward from the interface, *J(t|X, D)*, is proportional to the gradient of *n*, and we apply the diffusion coefficient as the standard proportionality term at position *X*:

$$J(t|X,D) = D \cdot \frac{\partial}{\partial X} N(t|X,D) = \frac{\sqrt{D}}{\sqrt{4\pi t}} \cdot e^{-X^2/4Dt} \tag{4}$$

Next, suppose we have an idea of a mean value for the diffusion coefficient, *D*, but don't know how much it varies. Lacking that information, we apply a maximum entropy estimate for the variance assuming a mean value D_0.

$$p_d(D) = \frac{1}{D_0} \cdot e^{-D/D_0} \tag{5}$$

We can then integrate the concentration across the diffusion probability density function, and the solution reduces to:

$$J(t|X) = \int_0^\infty J(t|X,D)p_d(D)dD = \frac{1}{4\sqrt{t}} \cdot e^{-X/\sqrt{D_0 t}} \left(\sqrt{D_0} + \frac{X}{\sqrt{t}}\right) \tag{6}$$

We also need to consider that for a highly disordered layer, we should place a maximum uncertainty around the value of *X*.

$$p_x(X) = \frac{1}{x_0} \cdot e^{-X/x_0} \tag{7}$$

Once again we can apply a probability density function, this time to the flux, which marginalizes *X* according to the following integration:

$$J(t) = \int_0^\infty J(t|X)p_x(X)dX = \frac{D_0}{4} \cdot \left(\frac{1}{x_0 + \sqrt{D_0 t}} + \frac{x_0}{(x_0 + \sqrt{D_0 t})^2}\right) \tag{8}$$

As a last step, we need to integrate the average flux over time to arrive at the growing width, *W*, of the oxide layer:

$$W(t) = \int_0^t J(\tau)d\tau = \frac{1}{2}\sqrt{D_0 t} \cdot \frac{\sqrt{D_0 t}}{x_0 + \sqrt{D_0 t}} \tag{9}$$

The time integral of this flux is the accumulated concentration of material with a constant inflow of material (i.e. molecular or elemental oxygen) from the surroundings. By integrating the diffusional

response, we can demonstrate how the step input transiently supplies reactants to the growing interface. The second factor is the newly realized suppressive effect due to disorder. For small *t*, this compensates the lead term to provide a linear growth factor, which is the original heuristic in the Deal-Grove growth law.

In summary, we applied a two step maximum entropy estimation process to model the disorder in the growing oxide layer. Without any knowledge about the distribution of *D* and *X*, apart from asserting that they must exist, we applied the following series of transforms:

$$n(t,x|D) \xrightarrow{integrate} N(t|X,D) \xrightarrow{flow} J(t|X,D) \xrightarrow{average} J(t) \xrightarrow{accumulate} W(t) \tag{10}$$

This provides a diffusional response due to a continuously applied step concentration to model a growing thickness. For oxide growth, a step input of oxygen is supplied from one side of the interface, and the substrate supplies silicon atoms, see **Figure 2.** The figure below provides a model fit to recent data from a set of SiO_2 growth experiments.

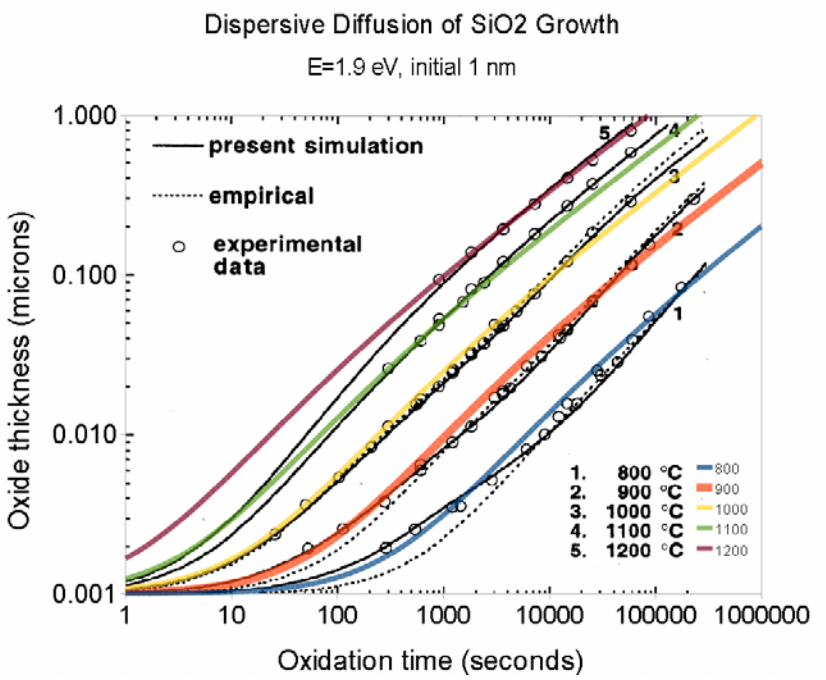

***Figure 3**: Comparison of dispersive diffusion model against the convention Deal- Grove model (empirical dotted) and a detailed simulation based on reaction kinetics. For silicon, an immediate oxide layer is formed which generates a baseline thickness of about 1 nanometer (data and simulation from [5])*

Over time, the response will attain a square root growth law, indicative of the Fick's law regime of what is often referred to as parabolic growth[1]. The larger the mean diffusion coefficient or the smaller the uncertainty level x_0, the more quickly that the response will diverge from the short-term linear growth regime.

[1] Parabolic growth is somewhat of a misnomer because the actual growth is a square root with time. In other words it is parabolic with respect to the growth distance.

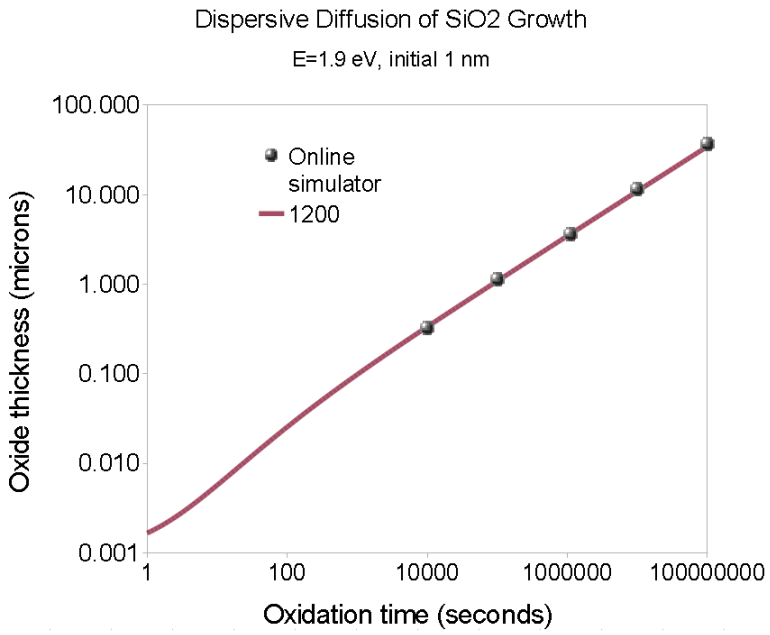

***Figure 4**: In the Fickian growth regime, the dispersive diffusion formulation follows a square-root time dependence, and can be confirmed with an online SiO_2 growth calculator*[2]

General Applicability

The uncertainty quantification proposed here has more general applicability than just to oxide growth on silicon. Any diffusional process that contains a degree of uncertainty in its parameters is a candidate for this simplification.

The general dispersed response to an impulse at the smeared origin is generated by the marginalization of Eq. 2 with Eq.5 and Eq.7 with the result:

$$\mathrm{n}(t) = \frac{2}{x_0 + \sqrt{Dt}} \tag{11}$$

This describes the damping of the peak concentration profile with time, cast in terms of a one-dimensional density. Alternatively, by scaling with a time constant, the impulse response can be normalized:

$$\mathrm{n}(t) = \frac{1}{1 + \sqrt{\frac{t}{\tau}}} \tag{12}$$

Here, τ is a diffusional time constant, indicating how slowly the concentration disperses from the origin. This is also a measure of the persistence of a material to remain localized (see [6]). The scaling implications are important to allow us to generalize the behavior over a range of conditions [7].

[2] Go to *http://www.cleanroom.byu.edu/ OxideThickCalc.phtml*

In fact, the dispersive formulation can extend to mathematically related behaviors such as corrosion and particulate growth. Corrosion acts very similar to oxidation in that the rate of the corrosive materials has to depend on diffusion of the reacting species with the replenishment of fresh substrate. Further, we can evaluate how well this applies to thermal diffusion, which uses the heat equation in a mathematical formulation very similar to particle diffusion.

Example: Thermal Dispersive Diffusion

The master model for thermal diffusion is referred to as the *heat equation*. This has the same formulation as Eq(1) with the role of material concentration played by temperature (which represents the local thermal excitation). In many practical applications, we may want to know the dissipation of heat from a source. In the case of a planar source of heat such as the surface of a CPU, we can use a one-dimensional model to illustrate the principle. Or we can demonstrate the flow of heat through a rod for different thermal conductivities (see **Figure 5**).

The ideal non-disordered impulse response should follow

$$\Delta T(t) = \frac{C}{\sqrt{Dt}} e^{\frac{-x^2}{Dt}} \tag{13}$$

The disordered variation of this is

$$\Delta T(t) = \frac{C}{\sqrt{Dt}} e^{\frac{-x}{\sqrt{Dt}}} \left(1 + \frac{x}{\sqrt{Dt}}\right) \tag{14}$$

Since each of the rods consists of a uniform homogeneous metal, one would expect that the response should be near to what theory predicts, and that is the case [8] .

For each of the materials of **Figure 5**, the idealized impulse response works well (Eq. 13), while the disordered variant (Eq. 14) reveals a larger dispersive spread.

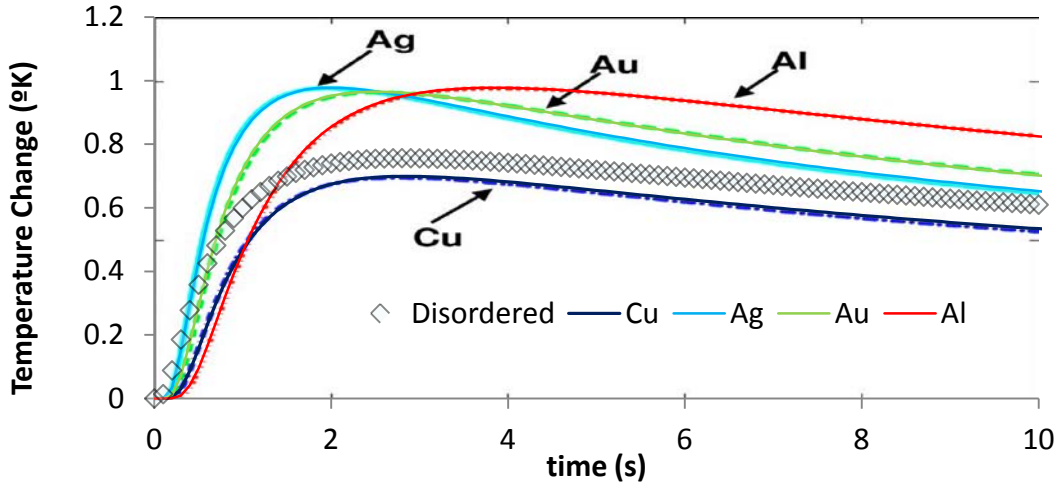

***Figure 5**: Experimentally measure thermal diffusion profiles for various metals showing excellent agreement with ordered diffusion. The dispersed diffusion profile is shown alongside.*

Where we would like to apply the disordered response is to an interface that has a thermal stimulus on one side and an outlet on the other, which turns out to be a realization of a compartmental or box model for thermal dynamics.

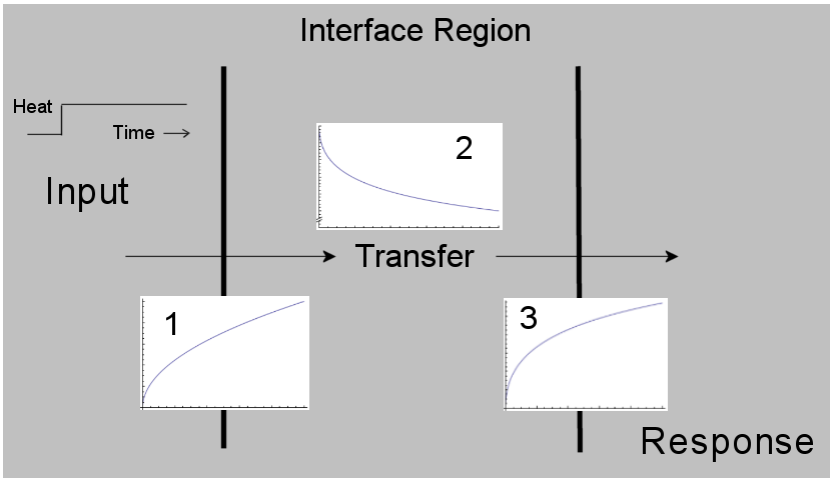

Figure 6: *A box model for thermal dynamics assumes a stimulus representing an initial transient (1) convolved against a dissipative transfer function (2) to produce a modulated response (3).*

The role of the box model is to model a thermal input along with a response which will allow an alternate path for dissipation of heat. In **Figure 6**, the input stimulus is a unit step which immediately creates a Fickian square root buildup near the interface (subgraph 1). This gets dissipated by a smeared impulse response function (subgraph 2) and the result is shown as a modulated response (subgraph 3) showing a slower buildup than the square root rise. The modulated reduction results from heat that is dissipated from non-specific paths as described in [8], described by **Figure 7**.

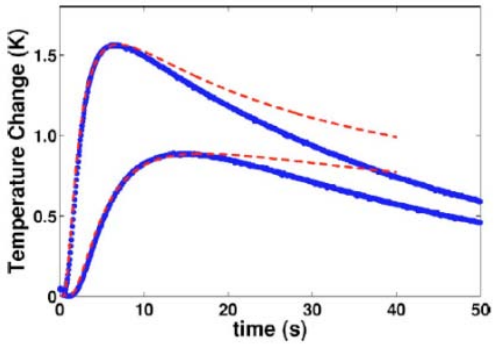

Figure 7: *Red lines indicate the theoretical profile under a non-lossy thermal environment.*

To analyze the thermal response we use the concept of a convolution to drive the response from a combination of input delta temperature change and the transfer function representing heat dissiation following secondary paths.

$$Response(t) = Input(t) \otimes Transfer(t) \tag{15}$$

At the origin of the thermal impulse, the smeared diffusive response is:

$$\Delta T(t) = \frac{1}{1 + \sqrt{t/\tau}} \tag{16}$$

This agrees with measurements from experiments, as shown in **Figure 8**.

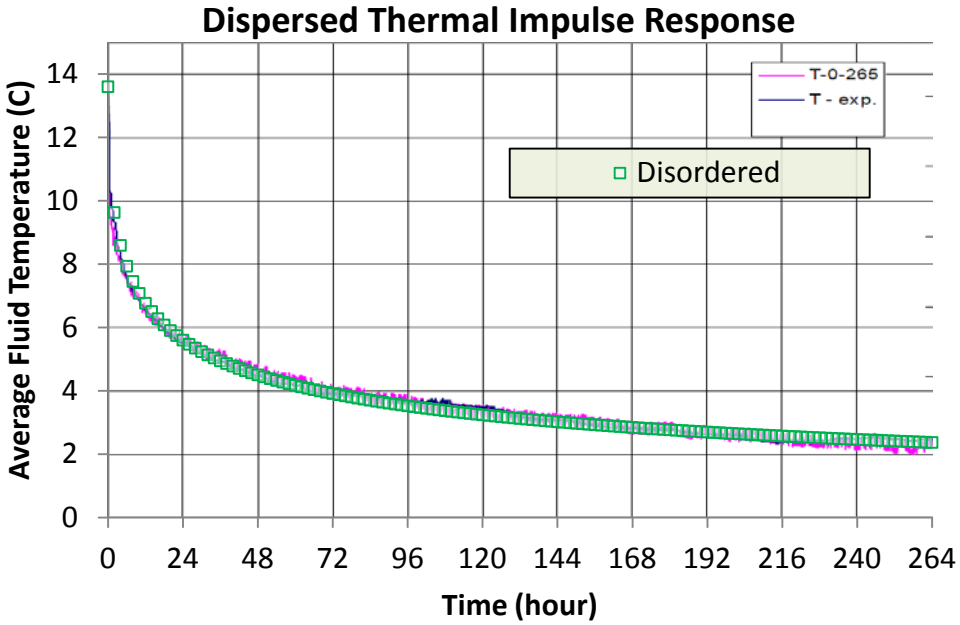

Figure 8: *Impulse response from a unit step thermal stimulus applied to an earthen mass (data from [9][10]).*

If we take a strong dispersive diffusive decline and convolve with a Fickian growth curve to model the loss:

$$Response(t) = \sqrt{t} - \sqrt{t} \otimes \frac{d}{dt}\left(\frac{1}{1 + \sqrt{t/\tau}}\right) \tag{17}$$

The result is a modulated response:

$$t > \tau \qquad Response(t) = \pi - \frac{2\,cosh^{-1}\left(\sqrt{t/\tau}\right)}{\sqrt{\frac{t}{\tau} - 1}} \tag{18}$$

$$t < \tau \qquad Response(t) = \pi - \frac{2\,cos^{-1}\left(\sqrt{t/\tau}\right)}{\sqrt{1 - \frac{t}{\tau}}}$$

A contour of the response surface is shown in **Figure 9**.

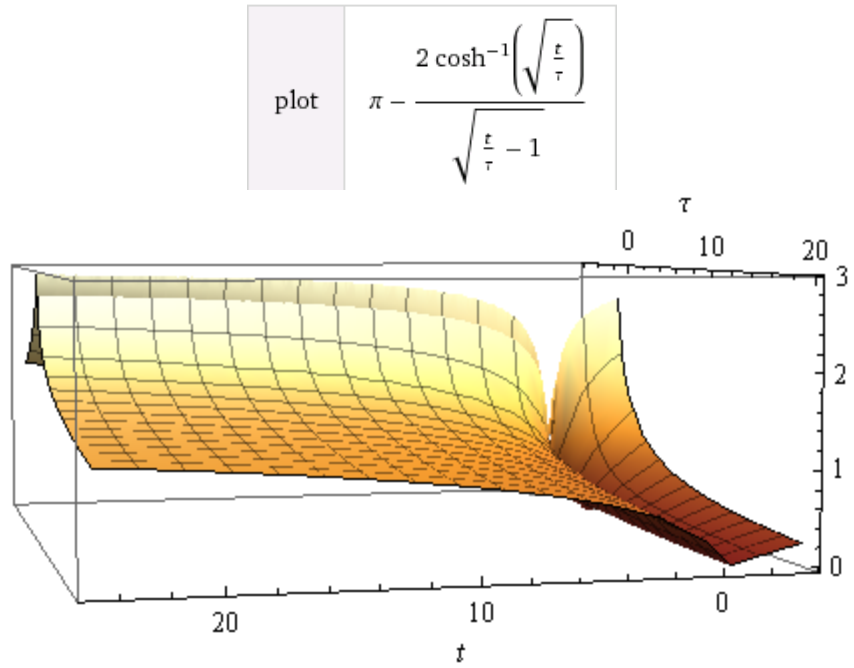

Figure 9: *Response surface of the dissipative dispersion function*

This formulation accounts for the dispersed heat losses arising from diffusion through dispersed paths.

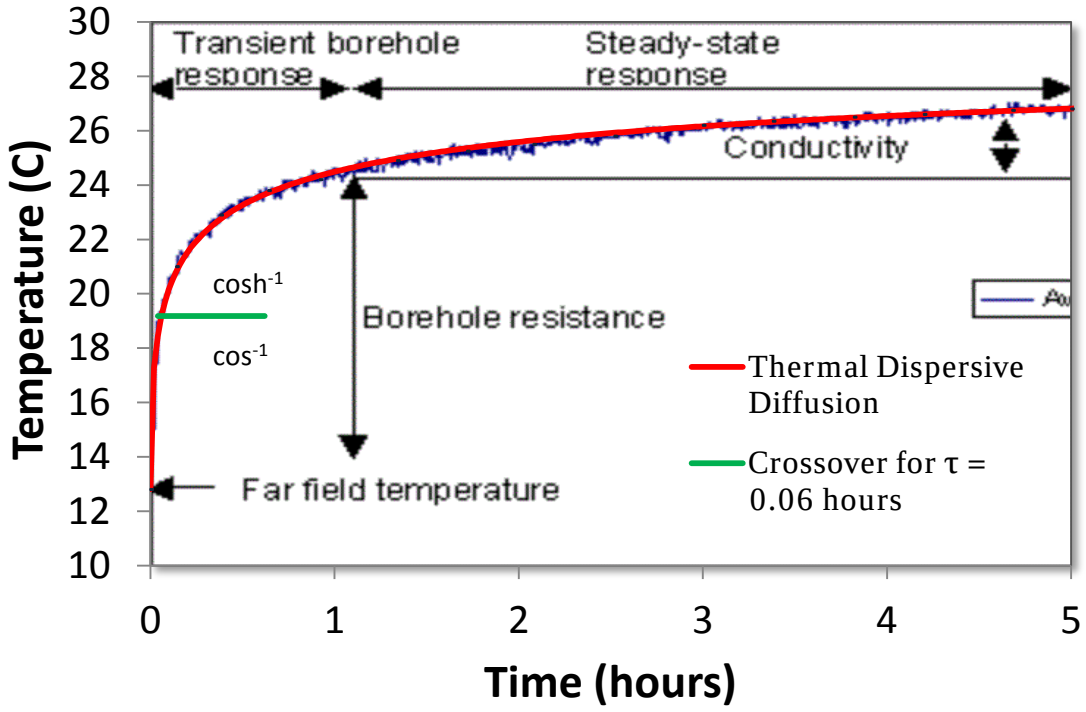

Figure 10*: Dispersed impulse response measured away from the stimulus. Note the crossover point separating the cosh $^{-1}$( ) and cos $^{-1}$ ( ) behavior (from [11]).*

By applying a sequence of thermal impulse steps we can demonstrate how to model piecewise transients (see **Figure 11**).

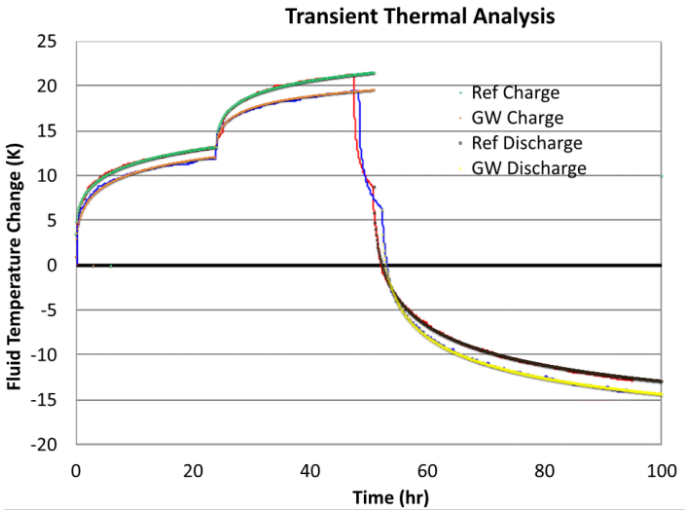

***Figure 11**: Series of hot and cold unit step impulses applied to an earthen mass measured as a transient response (data from [10] to a groundwater (GW) or reference sink.*

In addition to the utility for large scale geothermal transients as just described, we can also apply this dispersive thermal approach to smaller scale contexts, such as a component or subsystem heat sink. **Figure 12** shows typical thermal transients observed under various dissipation paths for a powered-up CPU card. Depending on whether the environment contains a well defined heat sink and cased enclosure, the transient will display markedly different apparent time constants. This by itself is not too surprising, but the dispersive diffusion response allows us a simple model to match up with the empirical results. In particular, where we have uncertainty in the environment, this approach excels, as it only requires a mean value estimate for the composite thermal diffusion coefficient or conductivity.

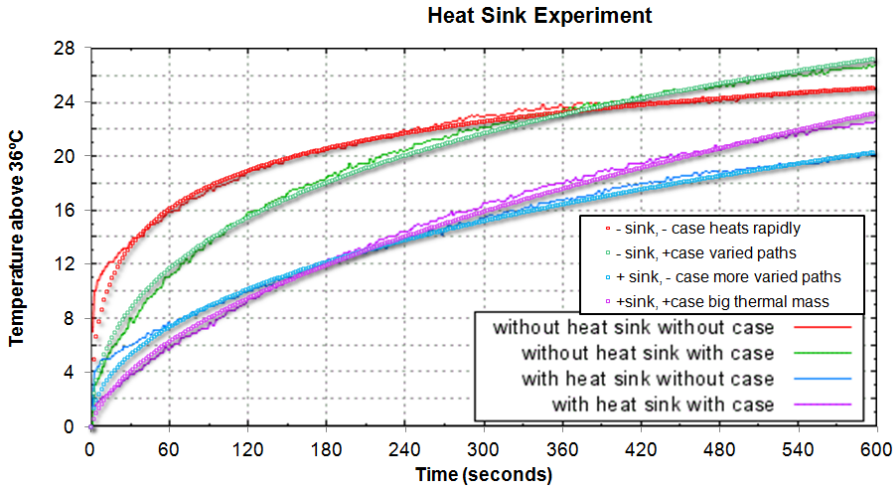

***Figure 12**: Thermal transients observed within a CPU housing.*

Example: Corrosive Growth

The salient principle behind the corrosion of metals is that rust growth mirrors that of the oxide growth of silicon. The number of random environmental factors involved in corrosion suggests that it would make an ideal candidate to apply the dispersive diffusion model. In the oxidation of steel, several different varieties of oxide are involved with varied atmospheric levels of corrosive reagents.

Figure 13 (linear scale) and **Figure 14** (log scale) show an oxide growth model and the results of experimental measurements for a steel composed structure left to weather under different climatic conditions. The behavior specified in Eq(7) was applied directly to the data with assumed mean values for an effective diffusion coefficient.

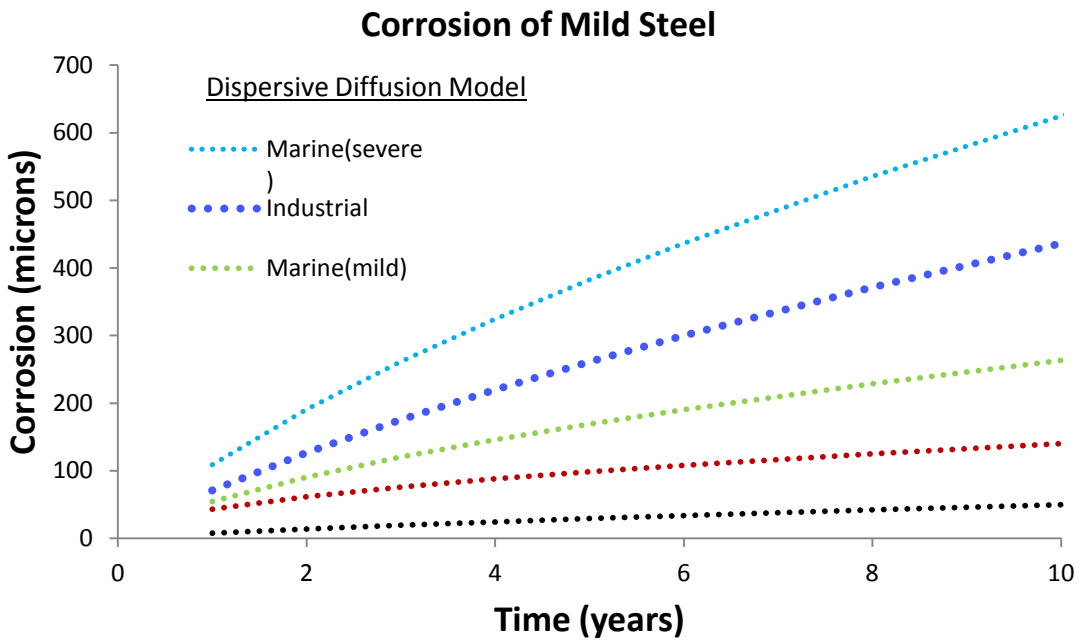

Figure 13: *Corrosion growth rates on a linear scale*

Uncontrolled rusting also has the propensity for peeling off thick layers, thus exposing fresh layers which will start the oxidation process over again. That tendency allows for the possibility for a growth power law of ½ combining with a linear growth law leading to the rough 0.7 power law observed. This is the same rate observed for the dispersive diffusion model with an uncertainty in the transition zone during the early oxidation process, see Eq(9) rewritten below with ***x*** representing the corrosion depth.

$$x(t) = \sqrt{Dt}\,\frac{\sqrt{\frac{Dt}{x_0}}}{1+\sqrt{\frac{Dt}{x_0}}} \tag{19}$$

The dynamic range is limited but the rate of growth suggests an initial linear regime, which then bends into the mixed power law growth of Eq(19). The model works well for the highly corrosive regimes of *marine* and *industrial* environments but diverges for the milder environments at longer times.

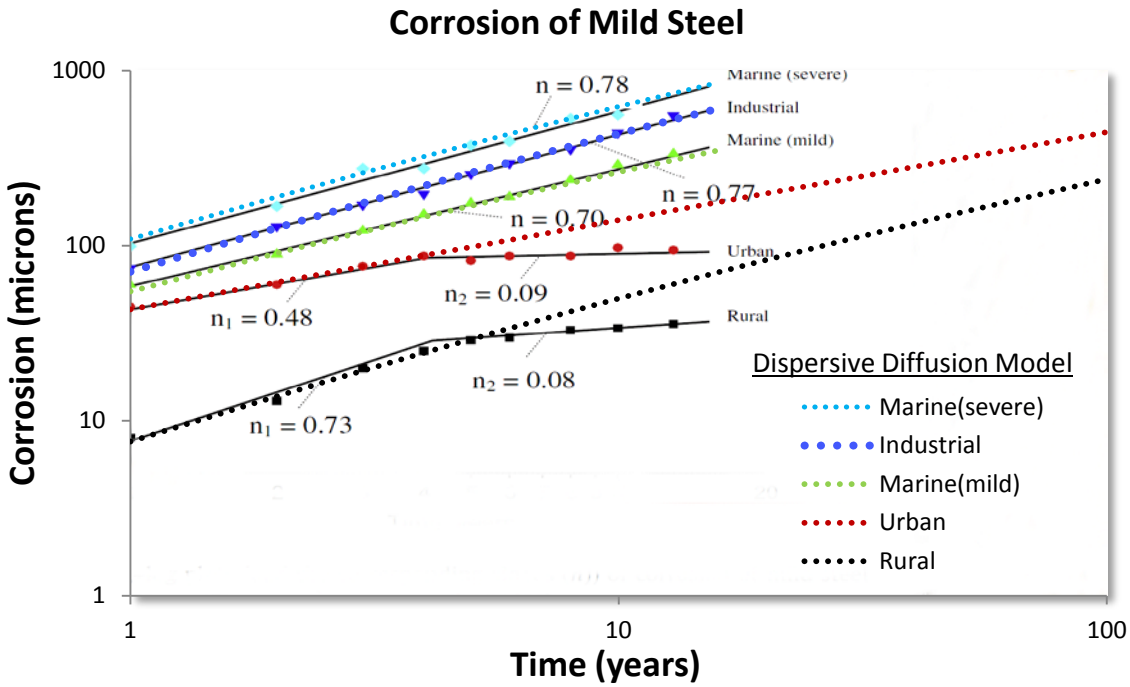

***Figure 14**: Corrosion growth rates on log scale compared against data from [12].*

Ornstein-Uhlenbeck correction: Due to its origins as a random walk process, a pure diffusion model of particles will show unbounded excursions given a long enough time duration. This is characterized by the unbounded Fickian growth law showing a $\sqrt{t}$ dependence for a pure random walk with a single diffusivity.

In practice, the physical environment of a particle may prevent unbounded excursions. It is physically possible that the environment may impose limiting effects on the extent of motion, or that it will place some form of drag on the particle's hopping rate the further it moves away from a mean starting value.

We can use the Ornstein-Uhlenbeck process to model mathematically how this pure random walk becomes bounded. The Ornstein-Uhlenbeck process has its origins in the modeling of Brownian motion with a special "reversion to the mean" property in motion excursions. The following expression shows the stationary marginal probability given a stochastic differential equation $dX = -a\,X \cdot dt + dW$ which models a drag on an excursion [13]

$$dP(X(t+s) = x \mid X(s) = 0) = \frac{1}{\sqrt{2\pi\tau}} e^{-\frac{x^2}{2\tau}}\, dx$$

$$where \quad \tau = \frac{1 - e^{-2at}}{2a}$$

The rationale for this limiting process to occur in a corrosive environment may arise from a barrier to diffusion beyond a certain critical thickness. As we demonstrated in volume 2 (see Appendix B), the Ornstein-Uhlenbeck process is very common at both gross and granular scales when it comes to describing terrain excursions, and the same process likely occurs at micro scales – perhaps occurring in a

similar fashion to when it was first formulated to describe Brownian motion in the presence of drag on particle velocities.

The O-U correction is straight-forward to apply on our dispersive corrosive growth formulation, we only need apply a non-linear transformation to the time-scale.

$$t \xrightarrow{O-U} \tau$$

and then apply this to the corrosion growth Eq(19):

$$x(\tau(t)) = \sqrt{D\tau(t)}\frac{\sqrt{\frac{D\tau(t)}{x_0}}}{1+\sqrt{\frac{D\tau(t)}{x_0}}} \xrightarrow{where} \tau(t) = (1-e^{-2at})/2a$$

This has the equivalent effect of appearing to slow down time at an exponential rate. This exponential rate turns out to be much faster than the Fickian growth law can sustain, so that an asymptotic limit is achieved in the diffusional or corrosive growth extent.

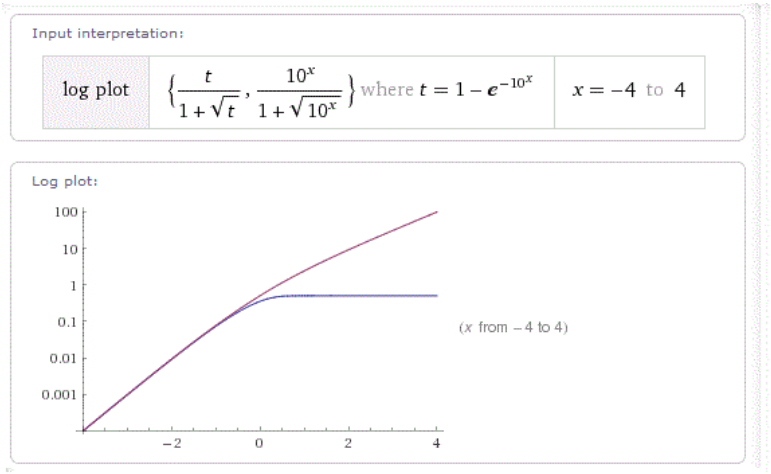

Figure 15: *The reversion to the mean process of the Ornstein-Uhlenbeck process will limit the growth of a diffusional process*

The caveat on this is that we are only applying this correction based on empirical observations. As an example, if the corrosion appears to flatten out as observed in the *urban* and *rural* rates of corrosion in **Figure 14**, we can model this behavior by assuming an Ornstein-Uhlenbeck reversion-to-the-mean process. In **Figure 16** below we apply the O-U limiting factor to model these two least corrosive environments.

As an explanation for a limiting effect on corrosive growth, it may be that a protective oxide — think in terms of something akin to the self-limiting growth of aluminum oxide Al_2O_3 — or perhaps some anodizing agent which forms after some time duration to limit further growth.

Whatever the rationale, the result of our characterization suggests that a rather simple formulation can be used to model the corrosive growth laws, with enough flexibility to handle the observed growth profiles.

Table 1: Parameterization for the corrosion model with Ornstein-Uhlenbeck reversion-to-the-mean drag, a.

	Marine(severe)	Industrial	Marine(mild)	Urban	Rural
D	90,000	45,000	12,000	6,800	5,300
X_0	600	400	100	50	500
a	1.00E-08	1.00E-08	1.00E-08	0.4	0.2

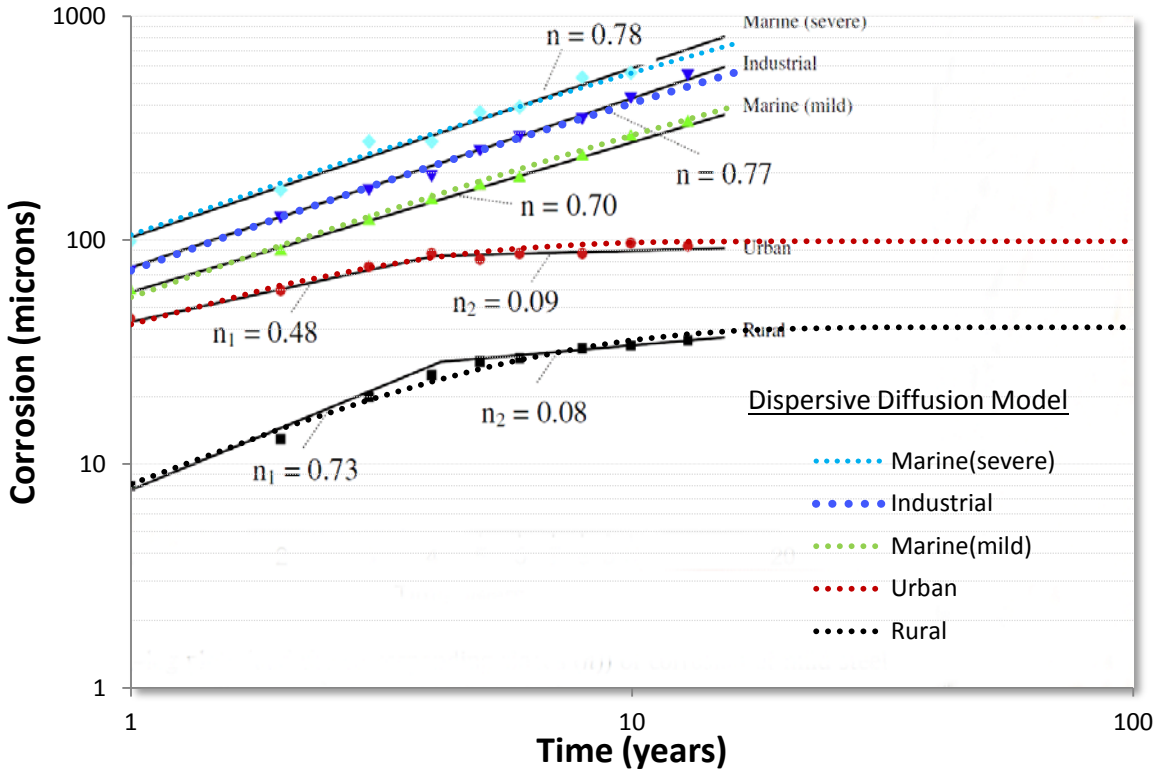

***Figure 16**: Model fits assuming the Ornstein-Uhlenbeck process. The urban and rural corrosion rates show a stronger asymptotic trend, indicating a reversion to the mean.*

In the following we consider examples on a larger scale which show the generality of the dispersion characterization technique and how Ornstein-Uhlenbeck process may apply.

Example : Diffusive Flow from Hydraulically Fractured Volumes

Recently, oil and natural gas extraction has shifted from conventional techniques to unconventional approaches as depletion of natural reserves sets in [6][14][15][16]. The replacement approaches rely on novel mechanisms to enhance the recovery of what is often referred to as *tight oil* within less-porous and permeable deposits of shale and limestone.

The most common technique involves the hydraulically-induced fracturing of shale deposits. The fracturing of shale into crevices and fissures allows the trapped oil and natural gas to escape along random seams to collection points along the horizontally aligned drilling path. **Figure 17** illustrates the

behavior that the trapped oil will show when released from the trapped state. As the fracturing reveals a random pattern of paths, the flow of oil will also reveal a random diffusional flow away from the regions of originally high concentration as it follows the random paths.

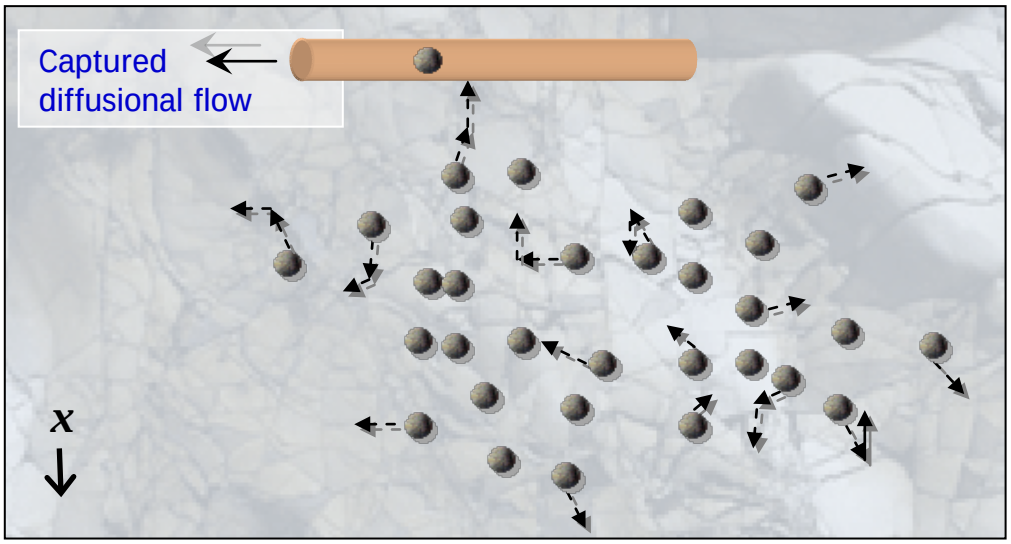

Figure 17 : *Diffusional Flow from fractured porous media*

The cross-sectional capture of oil is represented mathematically as the integrated flow of oil away from a dispersed volume of point sources. The uncertainty both in (1) the volumetric extent and (2) the variable diffusivity within a multiphase porous media, makes the analysis amenable to similar MaxEnt formulations used to describe diffusion-assisted oxide growth described earlier in this paper.

Figure 18 below shows the application of the dispersive diffusive flow derived in Eq. 12 to the cumulative production of a typical Bakken well [17]. The two parameters of the model, a median diffusion time and a scaling cumulative were adjusted to give the smallest residual error to the data.

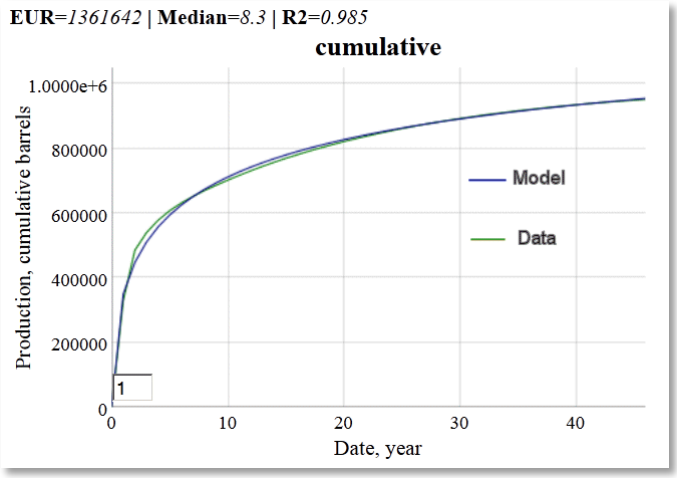

Figure 18*: Cumulative production from what is referred to as a typical hydraulically fractured well in the Bakken shale formation of North Dakota. The cumulative production was monitored as a function of time from the start of extraction.*

Not every well will show this good an agreement with the model (see the Annex for an independent and unbiased substantiation of the model fit), since what are referred to as "above ground" decisions can modulate the flow of oil, but in terms of a statistical average, this formulation can prove useful to estimate the *expected ultimate recovery* (EUR) of the typical well, after a few initial data points become available.

$$\mathrm{P}(t) = n_0 - n(t) = \frac{n_0}{1 + \sqrt{\frac{\tau}{t}}}$$

The model shown as Eq. 12 can be linearized to the following form, where *P(t)* indicates cumulative production and n_0 is the ultimate production:

$$\frac{1}{\mathrm{P}(t)} = \frac{1}{\mathrm{n_0}} + \frac{1}{\mathrm{n_0}} \cdot \sqrt{\frac{\tau}{\mathrm{t}}}$$

When plotted and a least-squares regression is applied, the value of the intercept generates the reciprocal of the EUR, as shown below:

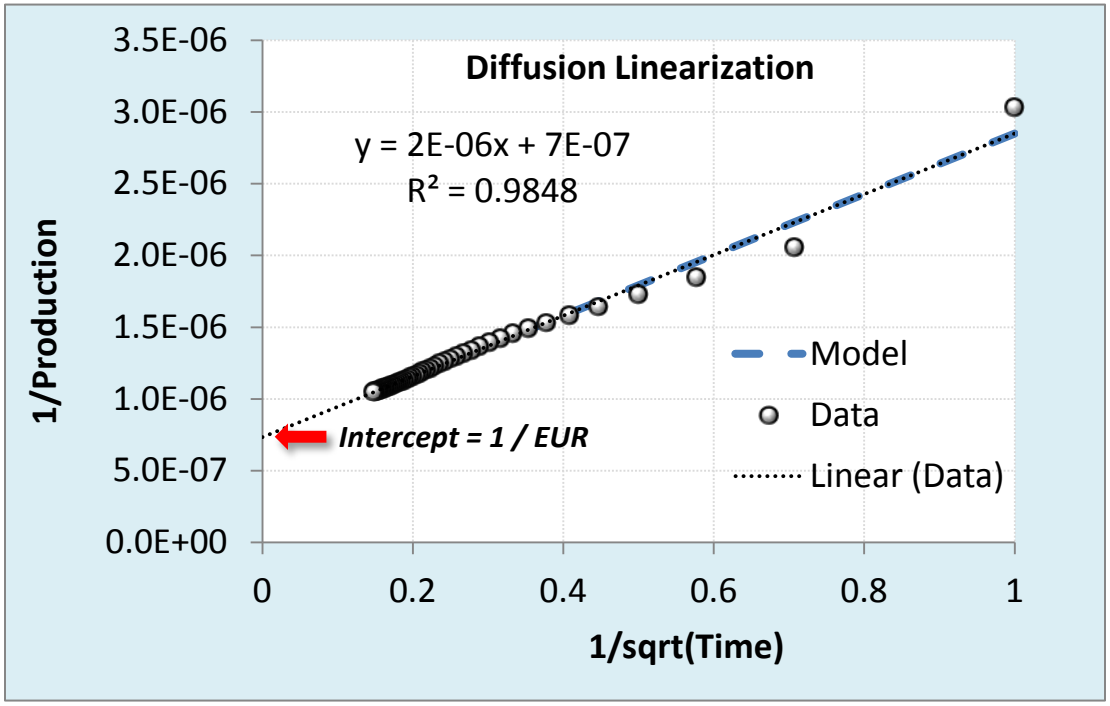

***Figure 19**: Linearization of diffusive model generates an estimate of ultimate recovery.*

Another "typical" well from the North Dakota Industrial Commission report [18] does not show as good agrement with the classical dispersed diffusion model (see **Figure 20**), but when Eq. 12 is modified by the reversion-to-the-mean characteristic of an Ornstein-Uhlenbeck process, the fit markedly improves while the expected cumulative is cut nearly in half in this particular case.

The drag-factor-limited diffusion in the O-U process essentially prevents the oil from traveling too far from its starting point, thus limiting the collection of oil at the well bore. The classical diffusion model thus provides an optimistic projection of ultimate recovery, while the O-U model generates a pessimistic

prediction. Unfortunately, the inflection point is only visible after a sufficient duration has elapsed, meaning that the linearization technique is not as effective.

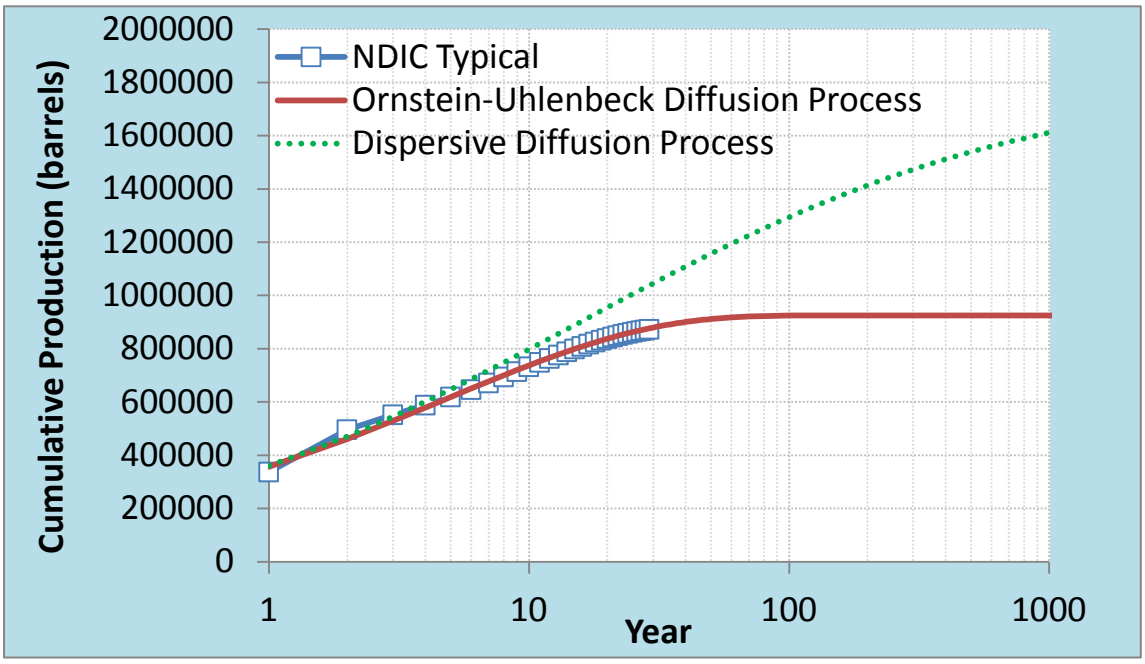

***Figure 20**: The Ornstein-Uhlenbeck process suppresses the diffusional flow by limiting the extent at which the mobile solute can travel, thus generating a constrained asymptote below that of drag-free diffusion.*

Besides oil, this model has applicability to hydrolically fractured natural gas production, as that it likely follows a similar diffusion process as for oxide and corrosion growth. This is a single impulse response profile. A typical decline curve from a set of shale gas wells is shown in **Figure 21** (see page 59 of [19]).

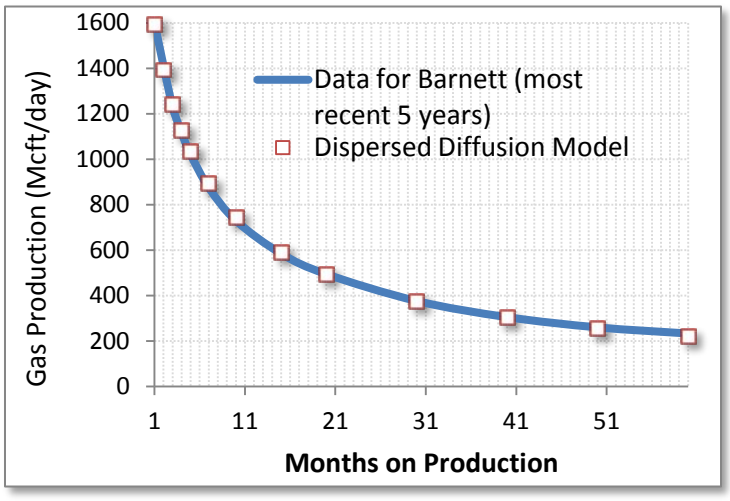

Data source

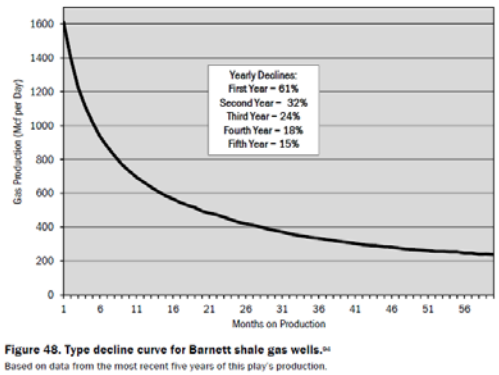

Figure 48. Type decline curve for Barnett shale gas wells.[64]
Based on data from the most recent five years of this play's production.

***Figure 21**: Typical decline curve for Barnett shale gas wells, based on the last five years of data from[19]. From the fit to the curve, production may have started on average 3 months prior to the first month plotted.*

The data source description states that the numbers were taken from the most recent 5 years of production. Since we do not know the start date, we add a term t_0 to indicate this uncertainty. The instantaneous production is the derivative of the cumulative:

$$p(t) = \frac{n_0}{2\sqrt{t - t_0}} \cdot \frac{\sqrt{\tau}}{\left(\sqrt{t - t_0} + \sqrt{\tau}\right)^2}$$

As a best fit, the median is 203 months or 16.9 years and t_0 is 3 months, with n_0 = 3.7 trillion ft^3.

The general trend described by the diffusive model is also supported by recent studies of shale gas located in the Barnett formation, where they report that "decline rate is the function of permeability, porosity and well depth and is proportional to $1/\sqrt{time}$" [20]. This agrees with the above formula for small times.

Petroleum engineers and geologists who specialize in fossil fuel reservoir modeling likely have similar analyses and heuristics (such as hyperbolic decline models) at their disposal, yet the dispersive diffusive model provides a useful explanation to the layman interested in future oil and natural gas supplies of a finitely constrained resource [6]. For example, the number of fractured wells showing a diffusive fall-off needed to keep up with demand leads to a *Red Queen* race of extraction activity [21][22][23].

Example : Diffusive Sequestering of Carbon Dioxide

The life-blood of the earth's biota is the carbon cycle. Elemental carbon resides in the land, aquatic, and atmospheric realms, and is continuously interchanged into various molecular forms as flora and fauna process other carbon-based lifeforms or extract what they can from the environment.

The addition of excess carbon into the atmospheric environment is not automatically handled by the biota, as they have been ecologically tuned to deal with the steady state value of around 280 to 300 PPM (parts per million) through gradual evolution and regional adaptation. This becomes a critical issue as the emitted carbon turns into carbon dioxide (CO_2) which acts as a greenhouse gas and can contribute to global warming and climate change[24][25]. **Figure 22** below estimates the gross amount of carbon emitted to the atmosphere over the years [26].

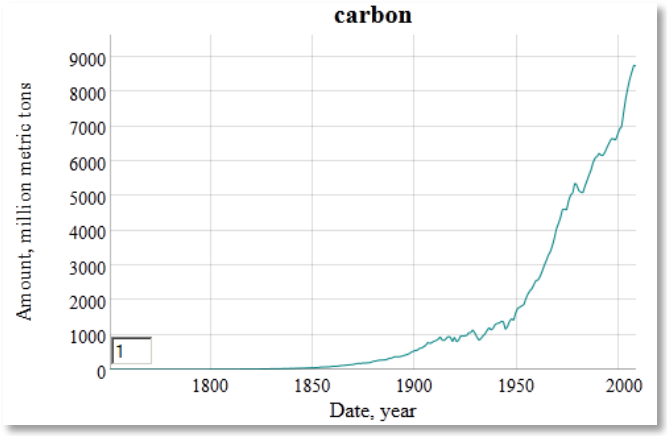

***Figure 22**: Industrial carbon outputs estimated since 1850, data supplied from [27]*

The estimated time it takes for CO2 to be sequestered has been modeled as a multiple-pathway mechanism, referred to as the Bern model [28][29]. By applying the same model we use for dispersive

diffusion we can align the somewhat complex Bern model with a relatively simple two-parameter equivalent as shown in **Figure 23** below. We also apply the Ornstein-Uhlenbeck limiting factor to emulate the strong negative drag to diffusional sequestering after 500 years. Diffusion and drag both contribute to the fat-tail that naïve first-order sequestering models ignore [30].

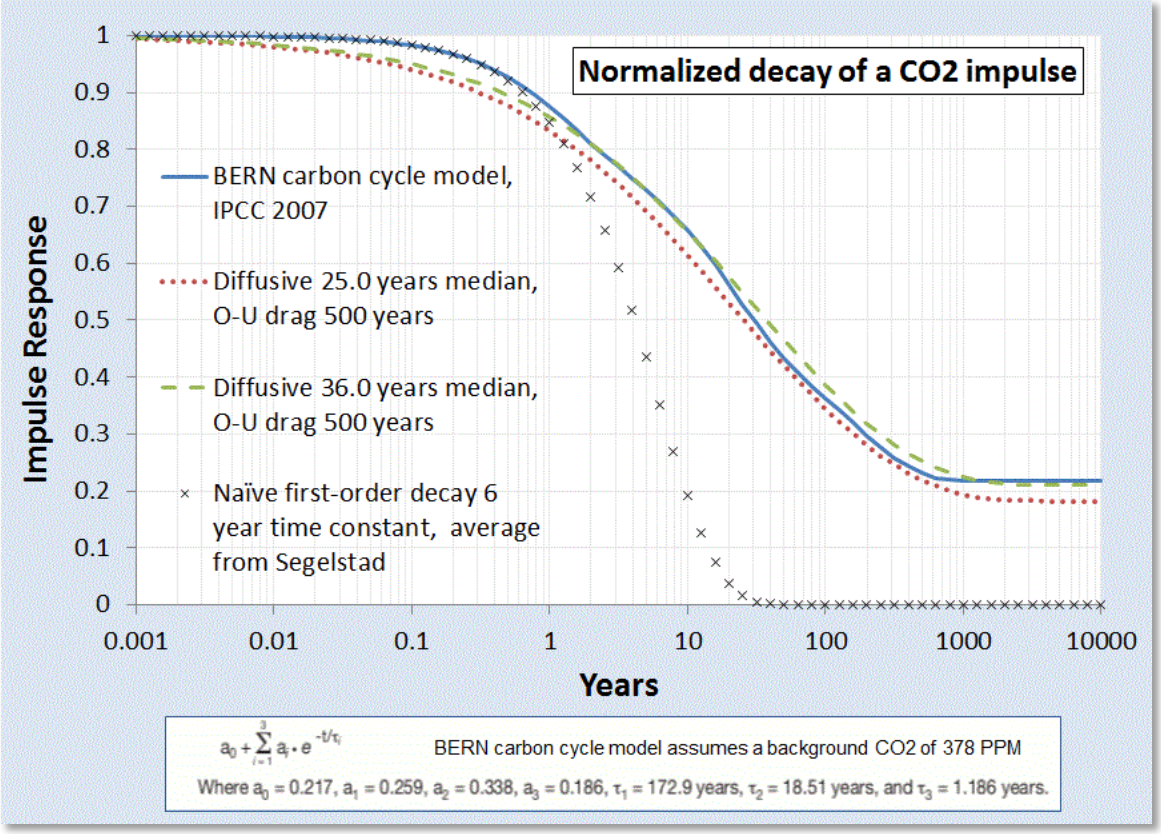

***Figure 23**: Impulse Response of the sequestering of Carbon Dioxide to a normalized stimulus. The solid blue curve represents the generally accepted model, while the dashed and dotted curves represent the dispersive diffsuion model*

The CO_2 evolution is mathematically descibed as the convolution of the carbon stimulus with the impulse response of CO_2 sequestering.

$$CO_2(t,T) = CO_2(0,T) + \kappa \int_0^t C(\tau) \cdot I(t-\tau) d\tau$$

The baseline CO_2 level has a temperature, *T*, dependence which reflects the seasonal and climatic changes. But apart from this factor, the large fraction of attributable increase of excess atmospheric CO results from the essential convolution of **Figure 22** and **Figure 23** along with a temperature dependence (0.21 eV solubility activation energy [31][32] and temperature data from [33]) which then produces **Figure 24**.

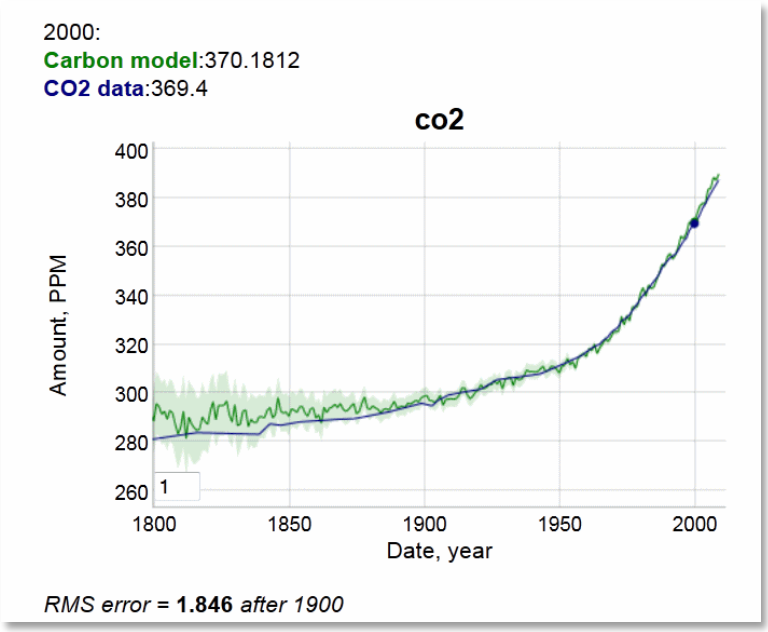

***Figure 24**: The remainder of CO_2 that is not sequestered by natural processes contributes to the excess atmospheric concentration measured by climatologists. The solid blue line is data derived from sensor readings from Mauna Loa since 1958 and patched with older historical records [34]*

The global concern that this model reveals is that the inertia to changes in carbon emission influence the excess CO_2 only gradually. Because of the fat-tail due to slow diffusional sequestering, the excess CO_2 will continue to build-up despite the cessation of emissions [35][6].

Example: Ocean Heat Content Model

The ocean heat content continues to increase and perhaps accelerate[36], as expected due to global warming. Much of the reduction in global temperature and especially land versus ocean surface temperatures results from significant heat sinking characteristics of the oceans[37].

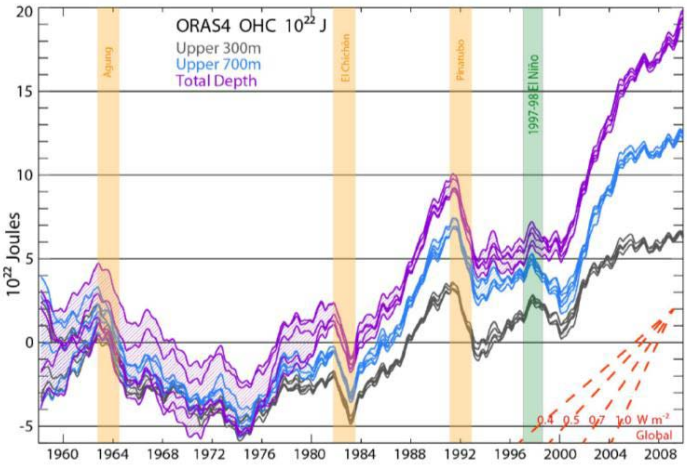

***Figure 25**: Ocean Heat Content from BTK [36]*

The objective is to create a simple model which tracks the transient growth as shown in the recent paper by Balmaseda, Trenberth, and Källén (BTK) [36] and described in **Figure 25.**

We will assume a diffusive flow of heat as described in J.Hansen's 1981 paper [2]. In general, the diffusion of heat is qualitatively playing out according to the way Fick's law would apply to a heat sink. Hansen also volunteered an effective diffusion that should apply, set to a round number value of 1 cm^2/second.

In the following we provide a mathematical explanation which works its way from first principles to come up with an *uncertainty-quantified* formulation. After that we present a first-order sanity check to the approximation.

We have three depths that we are looking at for heat accumulation (in addition to a surface layer which gives only a sea-surface temperature or SST). These are given as depths to 300 meters, to 700 meters, and down to infinity (or 2000 meters from another source [38]), as charted on **Figure 25**.

We assume that excess heat (mostly infrared from the greenhouse effect) is injected into the ocean's surface and works its way down through the depths by an effective diffusion coefficient. The kernel transient solution to the planar heat equation is given by Eq. 13. In this case *D* is the thermal diffusion coefficient, and *x* is the depth. The delta temperature is related to a thermal energy or heat through the heat capacity of salt water, which we assume to be constant through the layers. Any scaling is accommodated by the pre-factor, *c*

As a first level of uncertainty, we choose a *maximum entropy prior* and apply that to the diffusion coefficient to approximate the various pathways that heat can follow downward. For example, some of the flow will be by eddy diffusion, and other paths by conventional vertical mixing diffusion. If we apply a maximum entropy probability density function, assuming only a mean value for the diffusion coefficient as in Eq. 5 then we get the formulation of Eq. 14.

The next uncertainty is in capturing the heat content for a layer. The incremental heat across a layer depth, *L*, we can approximate as:

$$\int \Delta T(t|x)p(x)dx = \int \Delta T(t|x)\, e^{-x/L}\, dx$$

This results in the excess heat response, the following concise equation:

$$I(t) = \frac{\frac{\sqrt{Dt}}{L} + 2}{\left(\frac{\sqrt{Dt}}{L} + 1\right)^2}$$

This is also the response to a delta forcing impulse, but for a realistic situation where a growing atmospheric CO_2 concentration forces the response (explained in the previous example), we simply apply a convolution of the thermal stimulus with the thermal response. The temporal profile of the increasing aCO2 generates a growing thermal forcing function.

$$R(t) = F(t) \otimes I(t) = \int_0^t F(\tau)I(t-\tau)d\tau$$

If the thermal stimulus is a linearly growing heat flux, which roughly matches the GHG forcing function (see previous example)

$$F(t) = k \cdot (t - t_0)$$

Then, assuming a starting point $t_0 = 0$:

$$\frac{R(t)}{k} = \frac{2L}{3}(Dt)^{1.5} - L^2 Dt + 2L^3\sqrt{Dt} - 2L^4 \ln\left(\frac{\sqrt{Dt} + L}{L}\right)$$

A good approximation is to assume the thermal forcing function initiated approximately 50 years ago, circa 1960. We can then plot the equation for various values of the layer thickness, L, and a value of D = 2.5 cm^2/s, which is slightly higher than Hansen's model (which depends on the definition of diffusivity[3]). Values between 1.3 and 2.5 cm^2/s are used in other models [39].

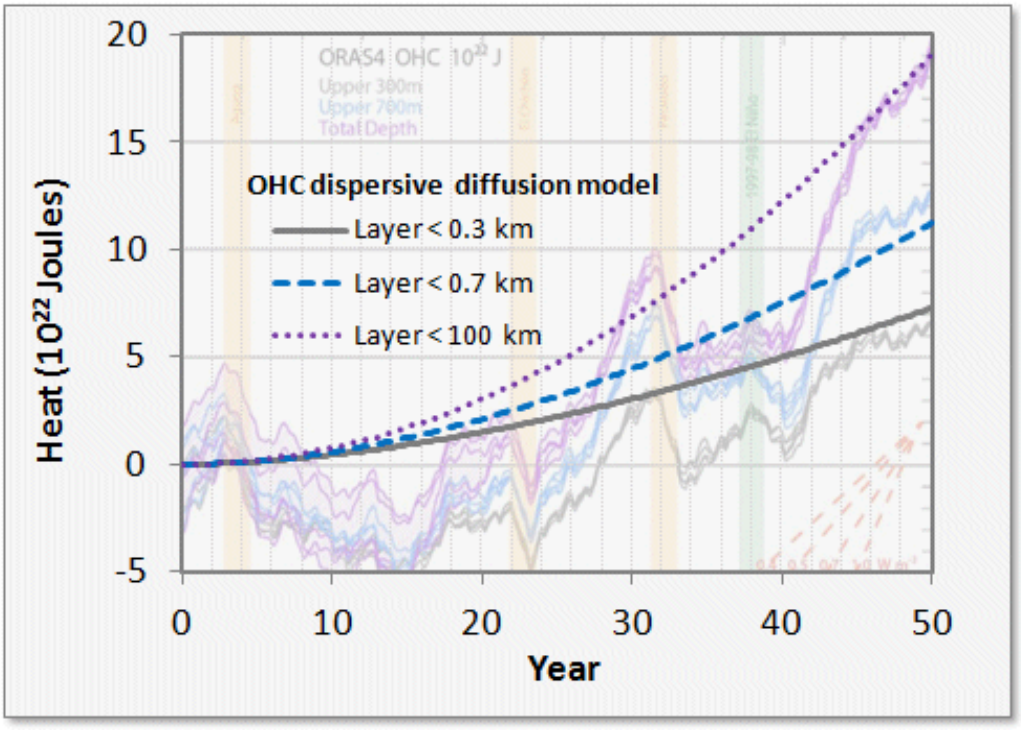

***Figure 26**: Thermal Dispersive Diffusion Model applied to the OHC data*

Another view of the OHC includes the thermal mass of regions that comprise the land, atmosphere and cryosphere regions (see **Figure 27**). This data appears smoothed in comparison to the raw data of **Figure 26**.

An alternate unstacked version of **Figure 27** is shown as **Figure 28** which is based on characterization of Levitus [40]. The dispersive diffusion models for the two depths are displayed as dashed green lines.

[3] Note that often a value of 2D instead of D is used in Eq. 13 depending on the definition of the random walk.

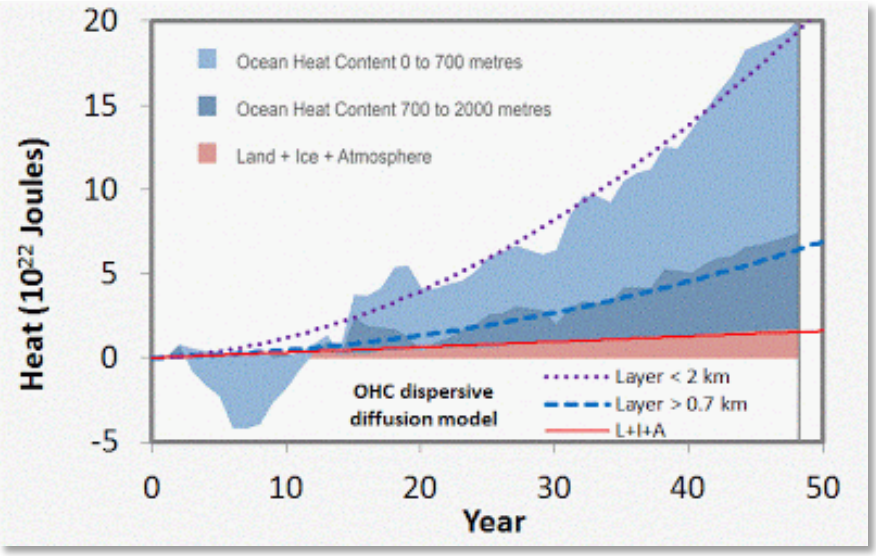

***Figure 27**: Alternate view of growing ocean heat content [38]. This also includes non-oceanic regions which generate a slightly increasing baseline.*

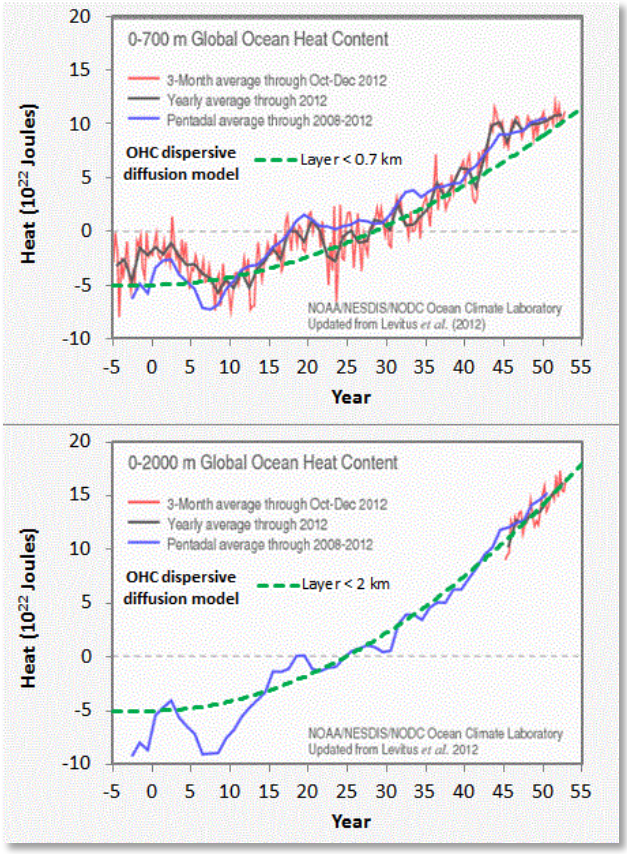

***Figure 28:** Non-stacked version of **Figure 27** (http://www.nodc.noaa.gov/OC5/3M_HEAT_CONTENT)*

In the latter figure, the agreement with the uncertainty-quantified theory is more striking. A single parameter, Hansen's effective diffusion coefficient *D*, along with the inferred external thermal forcing function is able to reproduce the temporal profile accurately.

The strength of this modeling approach is to lean on the maximum entropy principle to fill in the missing gaps where the variability in the numbers remains uncertain. In this case, the diffusion and ocean depths hold the uncertainty, and we use first-order physics to do the rest.

The following is a sanity check for the above formulation.

An application of Fick''s Law is to approximate the amount of material that has diffused (with thermal diffusion coefficient *D*) at least a certain distance, *x*, over a time duration, *t*, by

$$e^{-x/\sqrt{Dt}} = \frac{Q}{Q_0}$$

For greater than 300 meters, *Q/Q_0* is 13.5/20 read from **Figure 1**.
For greater than 700 meters, *Q/Q_0* is 7.5/20

Where *Q_0*=20 is the baseline for the total heat measured over all depths (i.e. between x=0 and *x*=infinite depth) reached at the current time. No heat will diffuse to infinite depths so at that point *Q/Q_0* is 0/20.

First, we can check to see how close the value of $L = \sqrt{Dt}$ scales, by fitting the *Q/Q_0* ratio at each depth.

For *x*=300 meters, we get *L*=763
For *x*=700 meters, we get *L*=713

These two are close enough to maintaining invariance that the Fick's law scaling relation holds and we can infer that the flow is by an effective diffusion [37].

We then use an average elapsed diffusion time of *t*=50 years and assume an average diffusion depth of 740, and *D* comes out to 3.65 cm^2/s. Hansen used an estimated value of diffusion of 1 cm^2/s, which is within an order of magnitude of this value and the value of 3 cm^2/s derived via temporal curve fitting.

This gives an approximate solution to the more general solution, which convolves an impulse function with a forcing function and watching that evolve according to **Figure 1** and **Figure 2** for the full temporal profile.

The analytical model assumes a ramped forcing function as a simplification of a more realistic effective forcing as described by Hansen [41]. Instead of using a ramp forcing function which gives the previous monotonically increasing analytical result, a realistic forcing (which takes into account perturbations due to volcanic events) is numerically convolved with the diffusive response function, *I(t)*.

Note that the volcanic disturbances are clearly visible in the response, although they do not show as sharp a transient decrease after the events, perhaps half of what **Figure 25** shows. The suppression due to the 1997-1998 El Nino is also not observable, but that of course is not an effective forcing and so would not be expected to appear in the convolution result.

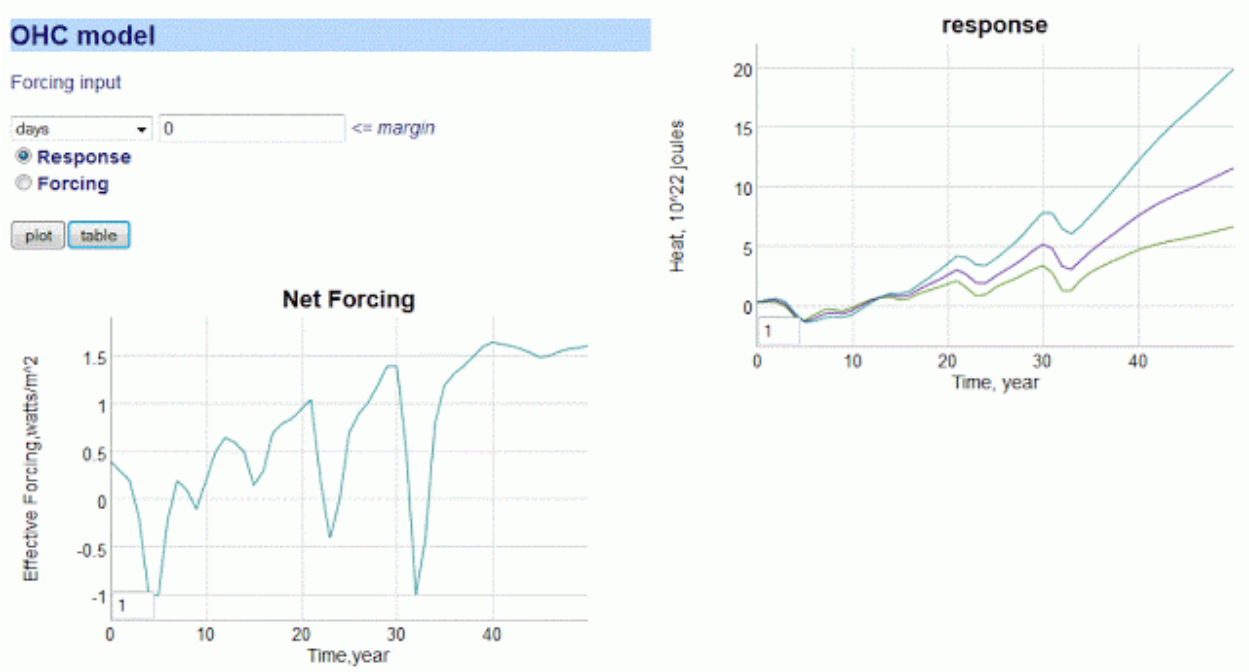

Figure 29: *Numerical convolution of effective forcing (lower left) is convolved with the diffusive transfer function to give the response (upper right). The three curves are < 300 m, < 700 m, and < 2000 m.*

Contrasting the early predictions of Hansen with the recent experimental measurements, we should note that nothing looks out of the ordinary for the OHC trending if we compare it to what conventional thermal physics would predict. The recent data has quantified the total heat absorbed along with cross-sectional estimates, which allows us to estimate the effective diffusion coefficient by evaluating how the heat contents vary with depth. We add a maximum uncertainty modifier to the coefficient to model the disorder in diffusivity (some of it eddy diffusivity, some open-ocean vertical, etc) and that allows us to match the temporal profile accurately.

Example: Dispersive Diffusion in Lithium-Ion Batteries

Modern rechargeable battery technology still relies on the principles of electro-chemistry and a reversible process, which hasn't changed in fundamental terms since the first lead-acid battery came to market in the early 1900's. What has changed is the combination of materials that make a low-cost, lightweight, and energy-efficient battery which will serve the needs of demanding applications such as electric and hybrid-electric vehicles (EV/HEV).

As energy efficient operation is dependent on the properties of the materials being combined, it is well understood that characterizing the materials is important to advancing the state-of-the-art (and in increasing EV acceptance).

Of vital importance is the characterization of diffusion in the electrode materials, as that is the rate-limiting factor in determining the absolute charging and discharging speed of the material-specific battery technology. Unfortunately, because of the competitive nature of battery producers, many of the characteristics are well-guarded and treated as trade secrets. For example, it is very rare to find diffusion

coefficient characteristics on commercial battery specification sheets, even though this kind of information is vital for optimizing battery management schemes [42][43].

In comparison to the relatively simple diffusional mechanisms of silicon oxide growth described earlier, the engineered structure of well-designed battery cell presents a significant constraint to the diffusional behavior. In **Figure 30** below we show a schematic of a single lithium-ion cell and the storage particles that charge and discharge. The disordered nature of the storage particles shown in the right figure is often described by what is referred to as a *tortuosity* measure [44] of local imperfections and inhomogeneities.

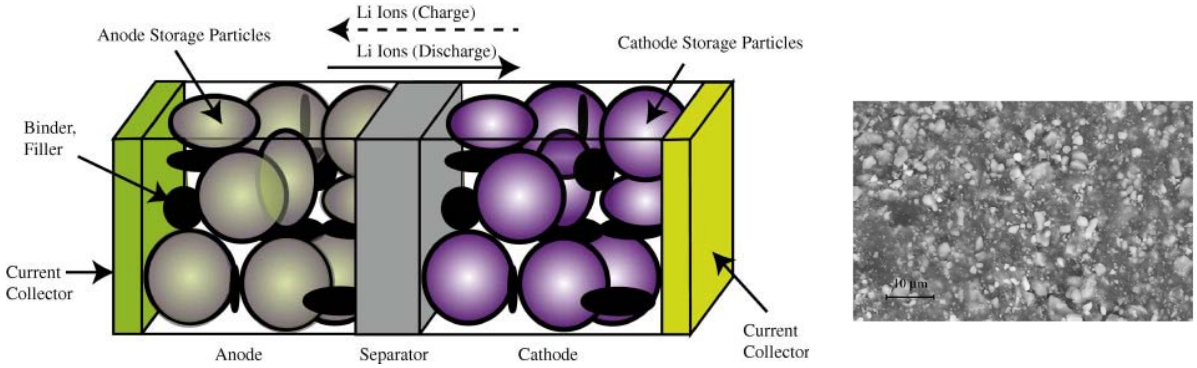

***Figure 30**: (Left) Exaggerated three-dimensional view of a lithium-ion battery cell and the direction of current flow during charging and discharging*
(Right) Realistic view of the heavily disordered nature of the $LiFePO_4$ storage particles [45].

The constraints on the diffusion limit the scale to that of the radius of the storage particle. The length scale is limited essentially to the values L to L_{max} shown in **Figure 31** below. The lithium -ion charge is spread throughout this particle and can only enter the electrolyte by diffusing outward from the inner region of this volume.

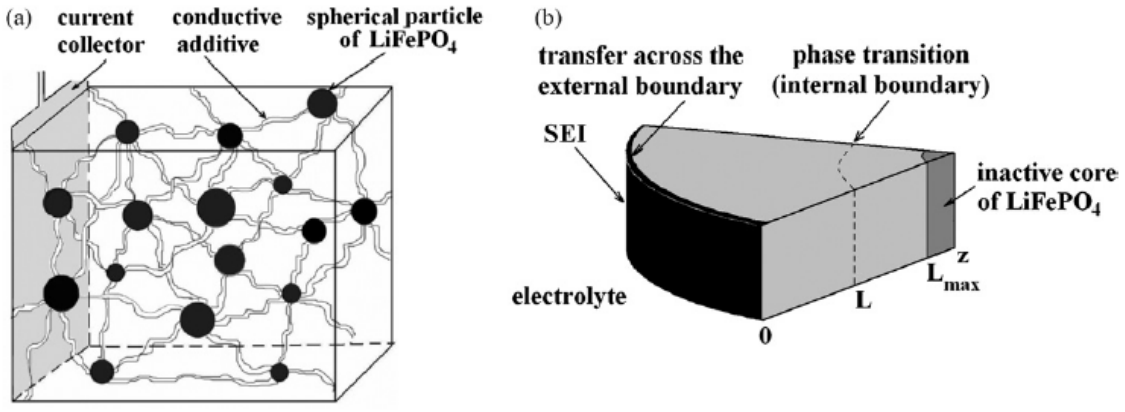

***Figure 31**: Diffusion of ions takes place through the radial shell of the $LiFePO_4$ spherical particle [1]. During the discharge phase, the ions need to migrate outward through shell and through the SEI barrier before reaching the electrolyte. At this point they can contribute to current flow [45].*

The size of the particles also varies as shown in **Figure 32** below. The two Lithium-ion materials under consideration, $LiFePO_4$ and $LiFeSO_4F$, have different materials properties but are structurally very similar (matrixed particles of mixed size) so that we can use a common analysis approach. This essentially

allows us to apply uncertainty in the diffusion coefficient and uncertainties in the particle size to establish a common diffusional behavior formulation.

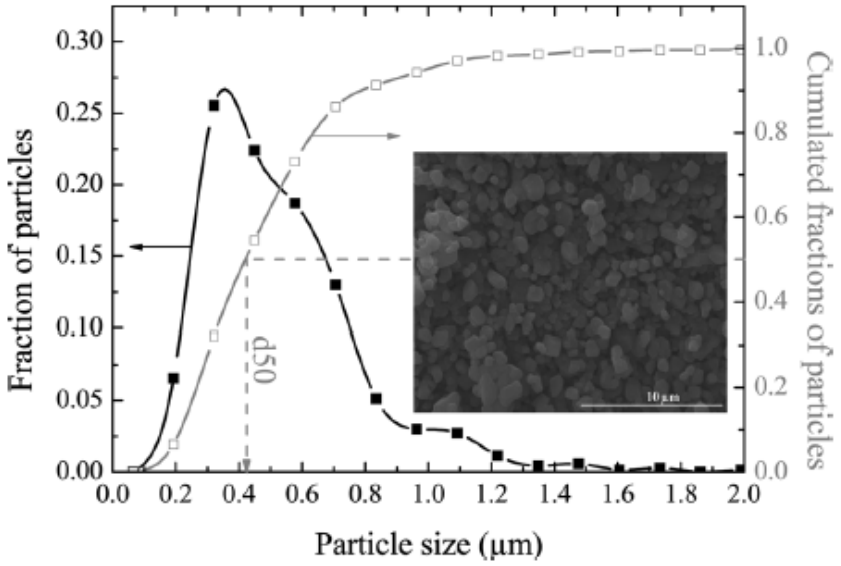

***Figure 32**: Particle size distribution of FeSO4F spherical granules [2]. The variation in lengths and material diffusivities opens the possibility of applying uncertainty quantification to a model of diffusive growth [46].*

Dispersive Diffusion Analysis of Discharging: The diffusion of ions through the volume of a spherical particle does have similarity to classical regimes such as the diffusion of silicon through silicon dioxide. That process (as described earlier in this paper) leads to the familiar Fick's law of diffusion, whereby the growing layer of oxide follows a so-called parabolic growth law with a thickness proportional to $\sqrt{time}$.

In a similar formulation that we used earlier for oxide and corrosive growth, the model that we can use for Li+ diffusion derives from the classic solution to the Fokker-Planck equation of continuity (neglecting any field driven drift).

$$\frac{\partial C}{\partial t} - D\nabla^2 C = 0$$

Here *C* is the lithium -ion concentration and *D* is the diffusion coefficient. Ignoring the spherical orientation of a particle, we can assume a solution along a radial one-dimensional outward axis, *x*:

$$C(t, x|D) = \frac{1}{\sqrt{4\pi Dt}}\, e^{-x^2/4Dt}$$

This is a marginal probability which depends on the diffusion coefficient. Since we do not know the variance of the diffusivity, we can apply a maximum entropy distribution across *D*.

$$p_d(D) = \frac{1}{D_0} e^{-D/D_0}$$

This simplifies the representation to the following workable formulation.

$$C(t,x) = \frac{1}{2\sqrt{D_0 t}} e^{-x/\sqrt{D_0 t}}$$

We now have what is called a kernel solution (i.e. Green's function) that we can apply to specific sets of initial conditions and forcing functions, the latter solved via convolution.

Fully Charged Initial Conditions
Assume the spherical particle is uniformly distributed with a charge density $C(0, x)$ at time $t = 0$.

Discharging Transient
For every point along the dimensions of the particle of size L, we calculate the time it takes to diffuse to the outer edge, where it can enter the electrolytic medium. This is simply an integral of the $C(t, x)$ term for all points starting from $x' = d$ to L, where d is the inner core radius from **Figure 31**.

$$C(t) = \int_d^L C(t, L-x)dx$$

This integrates straightforwardly to this concise representation:

$$C(t) = C_0 \frac{1 - e^{-(L-d)/\sqrt{D_0 t}}}{L-d}$$

The voltage of the cell is essentially the amount of charge available, so as this charge depletes, the voltage decreases proportionally.

We can test the model on two data sets corresponding to a $LiFePO_4$ cell [45] and a $LiSO_4F$ cell [46]. In **Figure 33** below, we show the model fit for $LiFePO_4$ as the red dotted line. This should be level-compared to the data designated by the solid black line labeled 1. The other curves labeled 2,3,4,5 are alternative diffusional model approximations applied by Churikov *et al* [45] that clearly do not work as well as the dispersive diffusion formulation derived above.

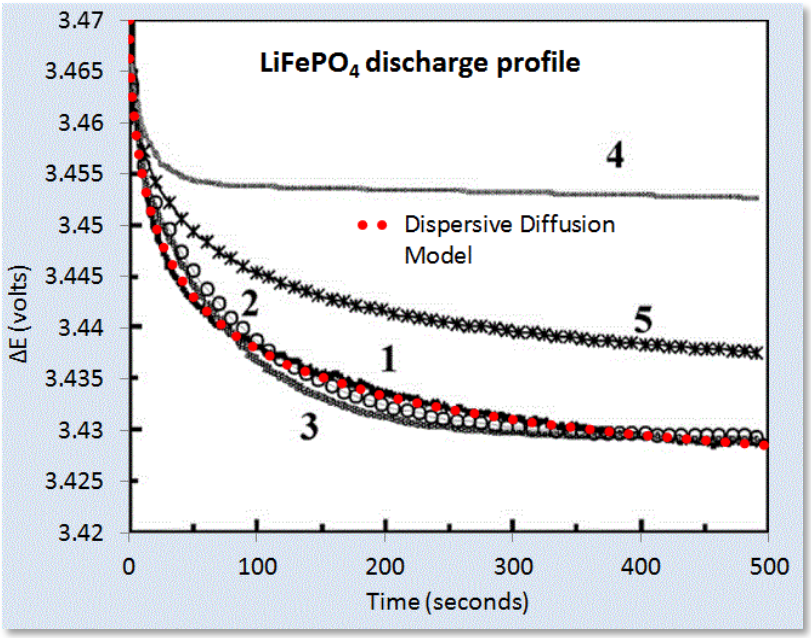

***Figure 33**: Discharge profile of LiFePO4 battery cell [45], with the red dotted line showing the parameterized dispersive diffusion model. The curves labeled 1 through 5 show alternative models that the authors applied to fit the data. Only the dispersive diffusion model duplicates the fast drop-off and long-time scale decline.*

Figure 6 below shows the fit to voltage characteristics of a $LiFeSO_4F$ cell, drawn as a red dotted line above the light gray data points. In this case the diffusional model by Delacourt [46]shown in solid black is well outside acceptable agreement.

Figure 34: Discharge profile of LiFeSO4F battery cell [46], with the red dotted line showing the parameterized dispersive diffusion model. The black curve shows the model that the authors applied to fit the data.

Constant Current Discharge

Instead of assuming that the particle size is fixed at *L*, we can assume that the *L* is an average value and apply the same maximum-entropy as a spread in sizes.

$$C(t) = \int_0^\infty C(t,x)\,\frac{1}{L}\,e^{-x/L}dx$$

This integrates straightforwardly to this concise representation, similar to that used earlier to describe oxide and corrosive growth:

$$C(t) = C_0\,\frac{1}{L+\sqrt{D_0 t}}$$

In addition to perhaps act as a better model of the disorder, the reason we do this is to allow us to recursively define the change in charge to a current. In this case, to get current we need to differentiate the charge with respect to time.

$$I(t) = \frac{dC(t)}{dt}$$

This differentiates to the following expression

$$I(t) = -\frac{C_0}{(L+\sqrt{D_0 t})^2}\,\frac{1}{2\sqrt{t}}$$

But note that we can insert *C(t)* back in to the expression

$$I(t) = \frac{C(t)}{(L+\sqrt{D_0 t})2\sqrt{t}}$$

Finally, since *I(t)* is a constant and we can set that to a value of $I_{constant}$. Then the charge has the following profile:

$$C(t) = C(0) - k_c I_{constant}(L+\sqrt{Dt})2\sqrt{t}$$

Or we can represent it as a voltage decline since stored charge is proportional to voltage:

$$V(t) = V(0) - k_v I_{constant}(L+\sqrt{Dt})2\sqrt{t}$$

For a set of constant current values, we can compare this formulation against experimental data [47] for $LiFePO_4$ (shown as gray open circles) shown in **Figure 35** below. A slight constant current offset (which may arise from unspecified shunting and/or series elements) was required to allow for the curves to align proportionally. Even with that, it is clear that the dispersive diffusion formulation works better than the conventional model (solid black lines) except where the discharge is nearing completion as it depletes the initial storage of charge.

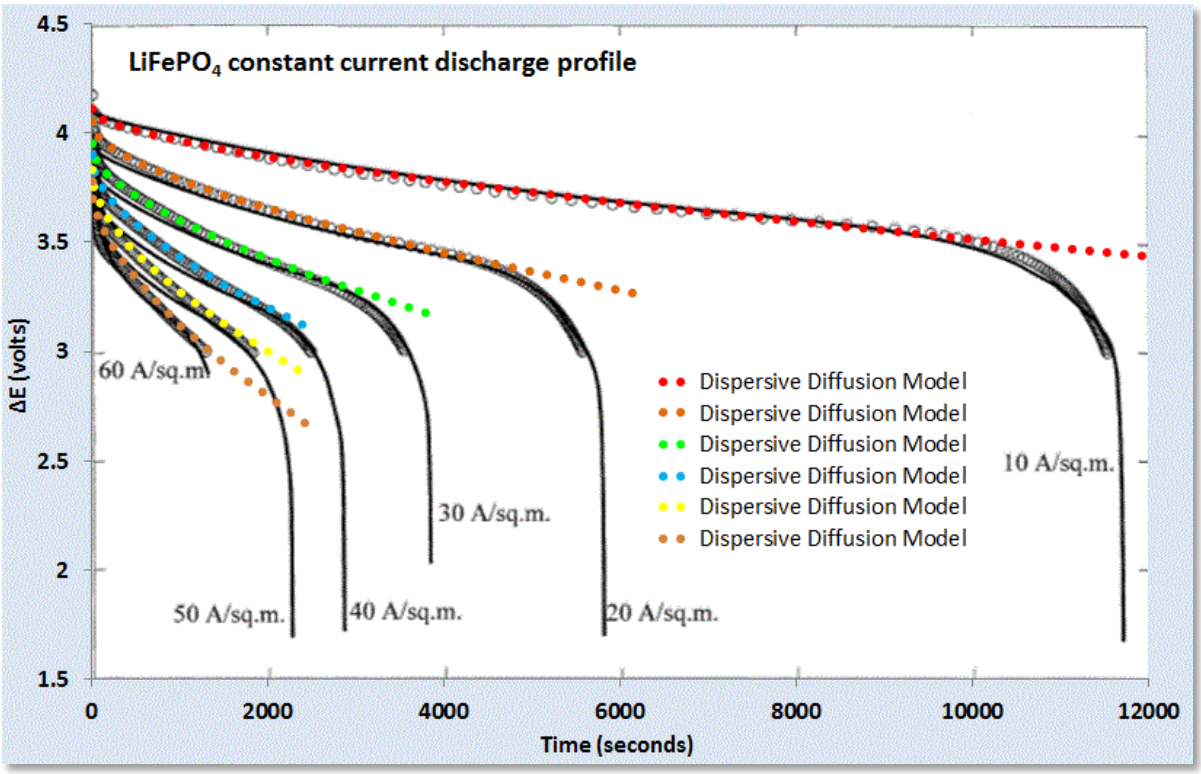

***Figure 35**: Constant current discharge profile [47]. Superimposed as dotted lines are the set of model fits which use the current value as a fixed parameter.*

The question is why does this simple formulation work so well for these open circuit and constant current discharge profiles? As with many similar cases of characterizing disordered material (see e.g. dispersive transport in photovoltaic semiconductors [6]), the fundamentally derived solution needs to be adjusted to take into account the uncertainty in the parameter space. However, this step is not routinely performed for battery models (see for example [48]) ; and adding modeling details to try to make up for a initially poor fit works only as a cosmetic heuristic. In contrast, by performing the uncertainty quantification on a simplified model, as done here by stochastically varying the diffusion coefficient and particle size, the first-order solution works surprisingly well with less need for the additional detail.

We can also model battery charging [49] but the lack of information on the charging profile makes the discharge behavior a simpler study, and one that demonstrates the application of dispersed diffusion and uncertainty quantification to a parametric model.

Conclusions

We have presented a series of physics-inspired models that approximate assorted diffusion phenomena well enough to be useful for model based engineering, providing significant advantages over both physical testing and reliance solely on data tables drawn from past testing. It should be noted that the question of when an approximate model is sufficiently accurate for a specific use depends upon the requirements that intended use places upon the model.

The statistician George E.P. Box wrote a famous quote concerning the validity of models. Box's oft-quoted statement of *"All models are wrong, but some are useful"* can be (and at times has been) misinterpreted. The original quote in full, drawn from the book "Empirical Model-Building and Response Surfaces" by Box and Draper, provides useful context:[50]

> "The fact that the polynomial is an approximation does not necessarily detract from its usefulness because all models are approximations. Essentially, all models are wrong but some are useful. However, the approximate nature of the model must always be borne in mind."

On the rest of that page, Box and Draper present a concise description of the differences between *epistemic* and *aleatoric* uncertainty, which is a crucial distinction for understanding the range of valid use for the models we present here. Epistemic uncertainties are the systematic errors (model uncertainty) that one can introduce in a statistical model, while aleatoric errors are those that are fundamental in the natural behavior itself (parametric uncertainty), be it noise or some other random effect.

The distinction between epistemic and aleatory uncertainty is central to understanding the scope of applicability of the oxide growth and thermal modeling described in this paper, and of the validity of environmental models in general. We can understand the basic mechanisms of oxide growth over many orders of magnitude via the parabolic Fickian diffusion law, but we may miss important details in how we choose to numerically model the fundamental equations. To remedy this situation, we treated the diffusion coefficient and the Si/SiO_2 interface location with the correct amount of aleatory uncertainty. Epistemic uncertainty remains potentially effecting the validity of the model we applied, which is addressed in accurately we can measure against the empirical observations.

The decision on whether a specific model is valid for a given use thus depends on how closely the problem at hand corresponds to data against which the model has been compared. Were the observational results and applicationidentical across available data sets, applying a sophisticated model, beyond a heuristic to match the data, would not be necessary. Repeatability leading to predicatibility is the key here, and that is why characterization in the semiconductor industry has been historically a critical factor in producing working chips.

If, on the other hand the case at hand is a serious extrapolation from past experience, careful consideration must be made of what effects the model may be neglecting and whether these effects could make the model's behavior misleading for the extrapolated case. Between the situations where a model is unnecessary and one where it is perhaps inappropriate (due to lack of information, etc), are a range of valid uses where the question at hand is how much error should be expected in model outputs. Our treatment of aleatory uncertainty provides a means to estimate expected error, when the question of model uncertainty has been appropriately addressed.

In that sense we can cast Box's phrase as essentially cautioning for appropriate care in determining appropriate use of models and for estimating numerical errors in statistical modeling. To interpret Box's quote as questioning the validity of using models in the first place would clearly be an incorrect argument — look at how far mathematical engineering based on models has gotten us! The Deal-Grove model

essentially allowed oxidation processes to become well characterized and predictable, which was central to revolutionizing the integrated circuit manufacturing process. The dispersive diffusion model derived in this paper should be taken in that spirit, a pragmatic model that could become useful in characterizing a fundamental physical process.

References

[1] J. Dunkel and P. Hänggi, "Relativistic Brownian motion," *Physics Reports*, vol. 471, no. 1, pp. 1–73, 2009.

[2] B. Baeumer, M. M. Meerschaert, and M. Naber, "Stochastic models for relativistic diffusion," *PHYSICAL REVIEW E Phys Rev E*, vol. 82, p. 011132, 2010.

[3] B. E. Deal and A. Grove, "General relationship for the thermal oxidation of silicon," *Journal of Applied Physics*, vol. 36, no. 12, pp. 3770–3778, 1965.

[4] U. Khalilov, E. C. Neyts, G. Pourtois, and A. C. T. van Duin, "Can We Control the Thickness of Ultrathin Silica Layers by Hyperthermal Silicon Oxidation at Room Temperature?," *The Journal of Physical Chemistry C*, 2011.

[5] M. Uematsu, H. Kageshima, and K. Shiraishi, "Microscopic mechanism of thermal silicon oxide growth," *Computational materials science*, vol. 24, no. 1, pp. 229–234, 2002.

[6] P. R. Pukite, *The Oil Conundrum: Vol. 1 Decline, Vol. 2 Renewal*, vol. 1,2, 2 vols. Daina, 2011.

[7] R. D'Almeida, S. Gonçalves, I. Baumvol, and F. Stedile, "Diffusion-reaction in thermal growth of silicon oxide films on Si," *Arxiv preprint cond-mat/9901335*, 1999.

[8] M. Sullivan, B. Thompson, and A. Williamson, "An experiment on the dynamics of thermal diffusion," *American Journal of Physics*, vol. 76, p. 637, 2008.

[9] H. J. L. Witte, G. J. van Gelder, and J. D. Spitler, "In Situ Meaurement of Ground Thermal Conductivity: The Dutch Perspective." [Online]. Available: http://www.groenholland.nl/download/Ashrae-108-1.pdf. [Accessed: 14-Mar-2012].

[10] H. Witte and A. van Gelder, "Geothermal Response Tests using controlled multipower level heating and cooling pulses (MPL-HCP): Quantifying groundwater effects on heat transport around a borehole heat exchanger," *Proc. Ecostock*, 2006.

[11] B. Groenholland, "Trial borehole & TRT - site testing & characterisation - Consultancy - Groenholland - Geo Energy Systems." [Online]. Available: http://www.groenholland.com/nl/consultancy/site_testing_and_characterisation/trial_borehole_and_trt.php. [Accessed: 29-Mar-2012].

[12] D. de la Fuente, I. Díaz, J. Simancas, B. Chico, and M. Morcillo, "Long-term atmospheric corrosion of mild steel," *Corrosion Science*, vol. 53, no. 2, pp. 604–617, Feb. 2011.

[13] D. Mumford and A. Desolneux, *Pattern Theory: The Stochastic Analysis Of Real-World Signals*. A K Peters, Ltd., 2010.

[14] D. L. Goodstein, *Out of gas: the end of the age of oil*. WW Norton & Company, 2005.

[15] J. A. Tainter and T. W. Patzek, "Our Energy and Complexity Dilemma: Prospects for the Future," in *Drilling Down*, Springer, 2012, pp. 185–214.

[16] D. Rutledge, "Estimating long-term world coal production with logit and probit transforms," *International Journal of Coal Geology*, vol. 85, no. 1, pp. 23–33, 2011.

[17] S. Nordeng, "North Dakota Department of Mineral Resources Three Forks 2012 Presentation," 15-Oct-2012. [Online]. Available: https://www.dmr.nd.gov/oilgas/presentations/EmmonsCoFB101512.pdf. [Accessed: 12-Mar-2013].

[18] D. Hvinden, "North Dakota Department of Mineral Resources Three Forks 2011 Presentation." [Online]. Available: https://www.dmr.nd.gov/oilgas/presentations/WBPC2011Activity.pdf. [Accessed: 12-Mar-2013].

[19] J. Hughes, "Drill,Bay,Drill : Can Unconventional Fuels Usher in a New Era of Energy Abundance?" [Online]. Available: http://www.postcarbon.org/reports/DBD-report-FINAL.pdf. [Accessed: 25-Feb-2013].

[20] S. Tinker, "Frequently Asked Questions (FAQ) – BEG Barnett Shale Assessment Study | JSG News," *Jackson School of Geosciences*, February 28, 20013. [Online]. Available: http://www.jsg.utexas.edu/news/2013/02/frequently-asked-questions-faq-beg-barnett-shale-assessment-study/. [Accessed: 05-Mar-2013].

[21] R. Likvern, "The Oil Drum | Is Shale Oil Production from Bakken Headed for a Run with 'The Red Queen'?"[Online]. Available: http://www.theoildrum.com/node/9506. [Accessed: 12-Mar-2013].

[22] Raymond Pierrehumbert, “U.S. shale oil: Are we headed to a new era of oil abundance? - Slate Magazine.” [Online]. Available: http://www.slate.com/articles/health_and_science/science/2013/02/u_s_shale_oil_are_we_headed_to_a_new_era_of_oil_abundance.html. [Accessed: 17-Feb-2013].
[23] D. Coyne, “peak oil climate and sustainability: Quick update to tight oil models.” [Online]. Available: http://oilpeakclimate.blogspot.com/2012/12/quick-update-to-tight-oil-models.html. [Accessed: 12-Mar-2013].
[24] A. A. Lacis, G. A. Schmidt, D. Rind, and R. A. Ruedy, “Atmospheric CO2: principal control knob governing Earth’s temperature,” *Science*, vol. 330, no. 6002, pp. 356–359, 2010.
[25] G. A. Schmidt, R. A. Ruedy, R. L. Miller, and A. A. Lacis, “Attribution of the present-day total greenhouse effect,” *Journal of Geophysical Research*, vol. 115, no. D20, Oct. 2010.
[26] T. Boden, B. Andres, and G. Marland, “Global CO2 Emissions,” *CDIAC*. [Online]. Available: http://cdiac.ornl.gov/ftp/ndp030/global.1751_2009.ems. [Accessed: 03-Mar-2013].
[27] DOE, “Carbon Dioxide Information Analysis Center (CDIAC).” [Online]. Available: http://cdiac.ornl.gov/. [Accessed: 12-Mar-2013].
[28] U. Siegenthaler and F. Joos, “Use of a simple model for studying oceanic tracer distributions and the global carbon cycle,” *Tellus B*, vol. 44, no. 3, pp. 186–207, 2002.
[29] J. Golinski, “Parameters for tuning a simple carbon cycle model,” *United Nations Framework Convention on Climate Change*. [Online]. Available: http://unfccc.int/resource/brazil/carbon.html. [Accessed: 12-Mar-2013].
[30] T. V. Segalstad, “Carbon cycle modelling and the residence time of natural and anthropogenic atmospheric CO2,” *BATE, R.(Ed., 1998): Global Warming*, pp. 184–219, 1998.
[31] J. J. Carroll, J. D. Slupsky, and A. E. Mather, “The solubility of carbon dioxide in water at low pressure,” *J. Phys. Chem. Ref. Data*, vol. 20, no. 6, pp. 1201–1209, 1991.
[32] L. W. Diamond and N. N. Akinfiev, “Solubility of CO< sub> 2 in water from− 1.5 to 100° C and from 0.1 to 100 MPa: evaluation of literature data and thermodynamic modelling,” *Fluid phase equilibria*, vol. 208, no. 1, pp. 265–290, 2003.
[33] BEST, “FAQ|Berkeley Earth,” *BERKELY Earth Surface Temperature*, 2013. [Online]. Available: http://berkeleyearth.org/faq/. [Accessed: 12-Mar-2013].
[34] KNMI, “Climate Explorer: Time series.” [Online]. Available: http://climexp.knmi.nl/getindices.cgi?WMO=CDIACData/co2_annual&STATION=CO2&TYPE=i&id=someone@somewhere&NPERYEAR=1. [Accessed: 08-Mar-2013].
[35] D. Archer, “Fate of fossil fuel CO2 in geologic time,” *Journal of Geophysical Research*, vol. 110, no. C9, p. C09S05, 2005.
[36] M. A. Balmaseda, K. E. Trenberth, and E. Källén, “Distinctive climate signals in reanalysis of global ocean heat content,” *Geophysical Research Letters*, 2013.
[37] J. Hansen, D. Johnson, A. Lacis, S. Lebedeff, P. Lee, D. Rind, and G. Russell, “Climate impact of increasing atmospheric carbon dioxide,” *Science*, vol. 213 (4511), pp. 957–966.
[38] D. Nuccitelli, R. Way, R. Painting, J. Church, and J. Cook, “Comment on ‘Ocean heat content and Earth’s radiation imbalance. II. Relation to climate shifts’,” *Physics Letters A*, vol. 376, no. 45, pp. 3466–3468, Oct. 2012.
[39] F. Joos, J. C. Orr, and U. Siegenthaler, “Ocean carbon transport in a box-diffusion versus a general circulation model,” *Journal of Geophysical Research: Oceans (1978–2012)*, vol. 102, no. C6, pp. 12367–12388, 1997.
[40] S. Levitus, J. Antonov, T. Boyer, O. Baranova, H. Garcia, R. Locarnini, A. Mishonov, J. Reagan, D. Seidov, and E. Yarosh, “World ocean heat content and thermosteric sea level change (0–2000 m), 1955–2010,” *Geophysical Research Letters*, vol. 39, no. 10, 2012.
[41] J. Hansen, M. Sato, P. Kharecha, and K. von Schuckmann, “Earth’s energy imbalance and implications,” *Atmospheric Chemistry and Physics*, vol. 11, no. 24, pp. 13421–13449, Dec. 2011.
[42] “Hybrid and Electric Vehicle Engineering Academy.” [Online]. Available: http://training.sae.org/academies/acad06/. [Accessed: 09-Jun-2013].
[43] M. Park, X. Zhang, M. Chung, G. B. Less, and A. M. Sastry, “A review of conduction phenomena in Li-ion batteries,” *Journal of Power Sources*, vol. 195, no. 24, pp. 7904–7929, Dec. 2010.
[44] D. Kehrwald, P. R. Shearing, N. P. Brandon, P. K. Sinha, and S. J. Harris, “Local tortuosity inhomogeneities in a lithium battery composite electrode,” *Journal of The Electrochemical Society*, vol. 158, no. 12, pp. A1393–A1399, 2011.

[45] A. Churikov, A. Ivanishchev, I. Ivanishcheva, V. Sycheva, N. Khasanova, and E. Antipov, "Determination of lithium diffusion coefficient in LiFePO< sub> 4 electrode by galvanostatic and potentiostatic intermittent titration techniques," *Electrochimica Acta*, vol. 55, no. 8, pp. 2939–2950, 2010.
[46] C. Delacourt, M. Ati, and J. Tarascon, "Measurement of Lithium Diffusion Coefficient in Li y FeSO4F," *Journal of The Electrochemical Society*, vol. 158, no. 6, pp. A741–A749, 2011.
[47] P. M. Gomadam, J. W. Weidner, R. A. Dougal, and R. E. White, "Mathematical modeling of lithium-ion and nickel battery systems," *Journal of Power Sources*, vol. 110, no. 2, pp. 267–284, 2002.
[48] J. Christensen and J. Newman, "A mathematical model for the lithium-ion negative electrode solid electrolyte interphase," *Journal of The Electrochemical Society*, vol. 151, no. 11, pp. A1977–A1988, 2004.
[49] Q. Wang, H. Li, X. Huang, and L. Chen, "Determination of chemical diffusion coefficient of lithium ion in graphitized mesocarbon microbeads with potential relaxation technique," *Journal of The Electrochemical Society*, vol. 148, no. 7, pp. A737–A741, 2001.
[50] G. E. P. Box and N. R. Draper, *Empirical model-building and response surfaces.* John Wiley & Sons, 1987.
[51] M. Schmidt and H. Lipson, "Distilling free-form natural laws from experimental data," *science*, vol. 324, no. 5923, pp. 81–85, 2009.

Annex

As a method to check the quality of fit for the diffusional formulation, we used an automated tool called ***Eureqa*** [51] to see if we could find better algebraic representations without biasing the solution space with contextual information. Given an *x-y* paired data set, ***Eureqa*** robotically searches the space of expressions, returning a penalty for either extra complexity (size) or excessive error (fit). The best solution is found on the Pareto-efficient frontier of these two factors. Shows the results, which by finding essentially the same hidden mathematical relationships in the raw data, substantiates the choice of the dispersive diffusion formulation. This is not proof of its validity, but it adds weight to our findings.

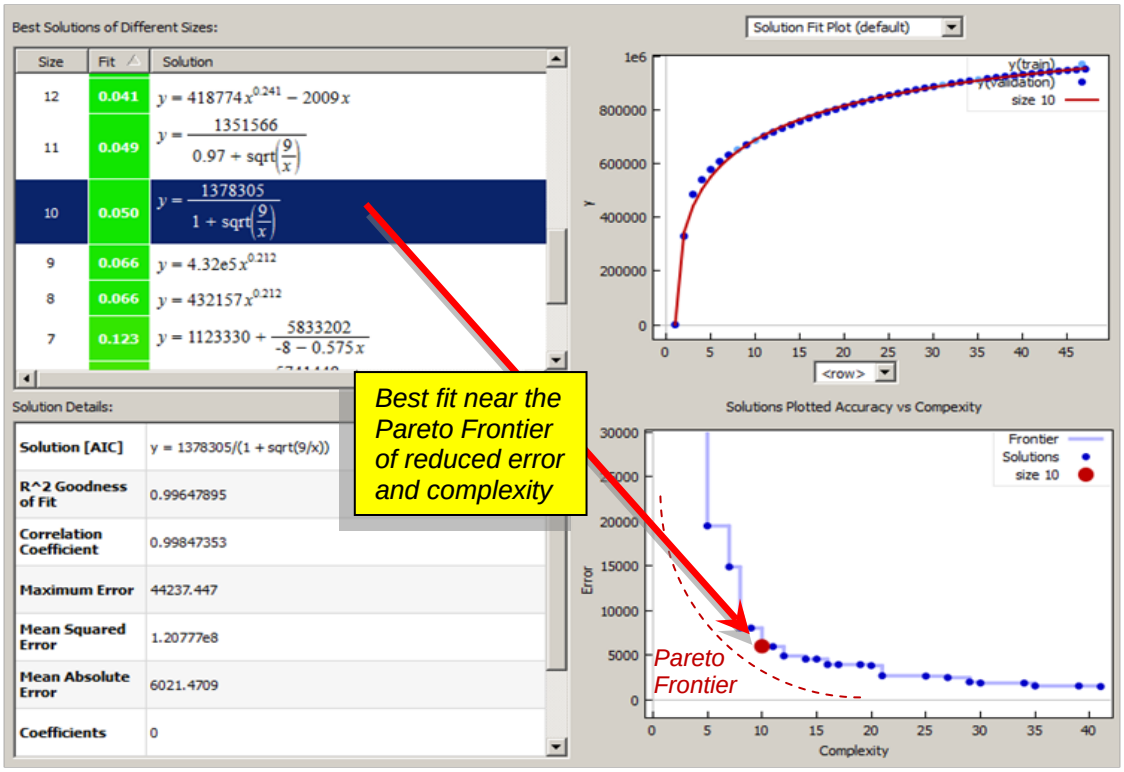

***Figure 36**: Using the Eureqa search tool, a factored solution very close to the dispersive diffusional formulation (highlighted as dark blue) was returned as the best fit along the complexity/error frontier*